

**Phase Resetting of Human Walking**

by

Daniel Klenk

S.B. Mechanical Engineering  
Massachusetts Institute of Technology

Submitted to the Department of Mechanical Engineering  
in Partial Fulfillment of the Requirements for the Degree of Master of Science in Mechanical  
Engineering

at the

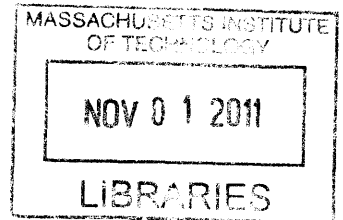
Massachusetts Institute of Technology

September 2011

© 2011 Massachusetts Institute of Technology. All rights reserved.

The author hereby grants to MIT permission to reproduce  
and to distribute publicly paper and electronics copies of this thesis document in whole or in part  
in any medium now known or hereafter created.

**ARCHIVES**



Signature of Author .....

Department of mechanical Engineering  
August 19, 2011

Certified by .....

Sun Jae Professor of Mechanical Engineering and Professor of Brain and Cognitive Sciences  
Thesis Supervisor

Accepted by .....

David E. Hardt  
Chairman, Depart Committee on Graduate Students

# **Phase Resetting of Human Walking**

by

Daniel Klenk

S.B. Mechanical Engineering  
Massachusetts Institute of Technology

Submitted to the Department of Mechanical Engineering  
in Partial Fulfillment of the Requirements for the Degree of Master of Science in Mechanical  
Engineering

## **Abstract**

This thesis is an investigation of the neural control of unimpaired human walking. Specifically, this work studied the potential for phase resetting of human walking by analyzing results from treadmill walking experiments. Subjects walked on a treadmill while wearing a robotic device that attaches to the lower leg, which applied 6 Nm torque perturbations to the ankle that acted to plantarflex the ankle. The effect of these perturbations on the stride period was then analyzed to determine the potential for phase resetting of the gait. For the experimental setup used, no phase resetting was found. This was determined by fitting a Fourier series regression to the data and finding very low  $R^2$  values for all subjects, ranging from 0.04 to 0.10, which implies that no underlying periodic curve exists in the data. This evidence of zero phase resetting is consistent with prior work that indicates some type of kinematic controller is present during walking.

Thesis Supervisor: Neville Hogan

Title: Sun Jae Professor of Mechanical Engineering and Professor of Brain and Cognitive Sciences

## **Acknowledgments**

I must first thank my advisor, Professor Neville Hogan, for devoting significant time and energy to my work. With his guidance, I have learned much about approaching a challenging problem and completing the proper analysis to generate a firm, conclusive answer. Professor Hogan's lucid explanations of various concepts have changed my perspective on engineering.

Next, I would like to thank Dr. Hermano Igo Krebs for raising many valuable questions during the course of this thesis. Pursuing these questions has improved my understanding of the problem at hand and the reasoning behind my answer.

I owe Joeeun Ahn many thanks for all of the helpful discussions concerning my work since the first day I began. I would also like to thank Hyunglae Lee and Panagiotis Artemiadis for numerous software consultations that greatly expedited my work.

Finally, I thank my parents for their support during these years, the importance of which I could never fully express. I would not have been able to pursue my desires in life without them.

## Table of Contents

Abstract.....	2
Acknowledgments.....	3
Table of Figures .....	5
Table of Tables .....	6
Table of Equations .....	6
Chapter 1 Introduction .....	7
1.1 Background on the Neural Control of Walking .....	7
Chapter 2 Phase Resetting Curves .....	8
2.1 Definition of phase .....	8
2.2 Phase Resetting .....	9
2.3 Phase Resetting Curves (PRC).....	9
2.3.1 Phase Resetting Curves: Theory and Applications.....	9
2.3.2 Computation of Experimental PRC's .....	10
Chapter 3 Experimental PRC of Human Walking.....	13
3.1 Subjects .....	13
3.2 Experimental Setup .....	13
3.3 Experimental Protocol.....	15
3.3.1 Warm-up: Finding the Preferred Walking Speed and Perturbation Demonstration.....	15
3.3.2 Data Collection: Walking with Perturbations.....	16
3.4 Data Analysis .....	17
3.4.1 Knee Brace Angle: Zeroing and Filtering .....	17
3.4.2 Footswitch Event and Poincaré Section Identification.....	17
3.4.3 Computing and Classifying the Stride Periods,.....	20
3.4.4 Computing the Intrinsic Stride Period and Verifying it is Constant.....	20
3.4.5 Verifying stride settling within two strides .....	22
3.4.6 Computing the phase shift .....	25
3.4.7 Plotting the PRC and a Least Squares Fourier regression .....	25
3.5 Results .....	26
Chapter 4 Discussion and Conclusions.....	32
4.1 PRC's for all Subjects were Indistinguishable from Zero.....	32

4.2 Considering the Potential for Artifact in the Zero PRC's .....	32
4.3 Interpretation of a Zero PRC for Human Walking.....	33
Bibliography .....	34
Appendix A: Stride Periods Plots .....	36
Appendix B: Knee plane plots sorted by perturbation phase.....	38
Appendix C: Histograms of perturbation distributions.....	56
Appendix D: Regression residuals ( $h = 10$ ).....	58

### Table of Figures

Figure 2.1 Stable limit cycle with two perturbations applied at different phases. The perturbed trajectories (dotted red) settle back to the limit cycle with a different phase when compared to the phase of the respective unperturbed trajectory (green). The perturbation at $\phi_2$ delays the phase, while the perturbation at $\phi_1$ advances the phase. ....	9
Figure 2.2 Limit cycle oscillator waveform plotted in time. The perturbation causes the perturbed trajectory to be delayed (negative phase shift), and the phase shifts are computed using the $\Delta t$ between the Poincaré section crossings. ....	11
Figure 3.1 Experimental setup. Subject on treadmill wearing the Anklebot with custom shoe and knee brace. ....	15
Figure 3.2 Example footswitch data with markers of four events: heel strike, heel off, toe strike, and toe off. ....	18
Figure 3.3 Footswitch data showing heel slap event used as a substitute for toe off. A toe off marker is shown at the heel slap events. ....	19
Figure 3.4 All stride periods for Subject 1, showing that the Stage 1 and 3 stride periods have a very similar distribution to that of Stage 2.....	21
Figure 3.5 All stride periods for Subject 8, which indicate that Stages 1 and 3 have different distributions than Stage 2, and thus Stages 1 and 3 are not usable for computing the intrinsic stride period. ....	21
Figure 3.6 Period-3 strides and Stage 1 unperturbed strides plotted in the knee plane for Subject 1. The Period-3 band of trajectories shows only slightly greater variability and was used as a valid representation of the limit cycle behavior.....	23
Figure 3.7 Period-3 knee plane plot and Stage1 unperturbed knee plane plot for Subject 8.....	23
Figure 3.9 Knee plane plot showing Period-1 trajectories perturbed between phases 0.9 – 1. All Period-2 strides have settled as all red dots lie inside the settled band. (Subject 1).....	24
Figure 3.10 Perturbation phase distribution for Subject 5. ....	25
Figure 3.11 Perturbation phase distribution for Subject 6. ....	25

Figure 3.13 Residuals for the regression fit for Subject 1 above. The absence of pattern in the residuals indicate that increasing the number of Fourier coefficients by increasing  $h$  will not improve the fit..... 27

Figure 3.15 PRC's: Subject 3,  $R^2 = 0.06$  (left) and Subject 4,  $R^2 = 0.06$  (right) ..... 29

Figure 3.16 PRC's: Subject 5,  $R^2 = 0.10$  (left) and Subject 6,  $R^2 = 0.07$  (right) ..... 30

Figure 3.17 PRC's: Subject 7,  $R^2 = 0.06$  (left) and Subject 8,  $R^2 = 0.04$  (right) ..... 30

Figure 3.18 PRC: Subject 9,  $R^2 = 0.05$  ..... 31

### Table of Tables

Table 3.1 Mean and standard deviation of physical characteristics and PWS (defined below) of experiment subjects..... 13

Table 3.2 The mean and standard deviation for all subjects' stride periods, showing the close agreement in stride period standard deviation of toe off vs. heel slap..... 20

**Table 3.3**..... 28

### Table of Equations

Equation 2.1 ..... 8

Equation 2.2 ..... 11

Equation 2.3 ..... 11

Equation 3.1 ..... 23

Equation 3.2 ..... 26

## **Chapter 1 Introduction**

### **1.1 Background on the Neural Control of Walking**

All animals have remarkable motor control capabilities thanks to an exceptional neural controller. In humans, significant progress has been made on understanding the motor control of the upper limb. However, control of the lower limb has many unanswered questions. Understanding the control of the lower limb, and more specifically the control of walking, has potential to improve our understanding of the challenges facing patients with neurological disease, so that effective rehabilitation therapy can be offered in an attempt to improve their mobility in everyday life.

Broadly speaking, there are two levels of controllers in the central nervous system that may be responsible for generating the rhythmic patterns of muscle signals that control walking in humans: supraspinal and spinal. Currently, the roles these neural controllers play in human walking is unknown. In animals, it is well established that neural circuits called central pattern generators (CPG's) lie in the spinal cord of numerous quadrupeds, including mammals and reptiles, which generate a complete, set of feedforward motor commands that can provide low level control of muscles for walking. These circuits can do so without any feedback, and require only a tonic, or "on/off" signal from the brain. This is not to say that the brain plays no role during walking in animals with CPG's, but rather serves to highlight the existence and role of such spinal CPG's in several types of animals.

For humans, it is still unknown whether CPG's exist in the spinal cord, and if so, exactly what role they play in the control of walking. There are many pieces of evidence that they do exist, but no clear answer is available. There is definitive evidence, however, that a nonlinear oscillator plays a role at some level in the control of walking. Such evidence is found in a study by (Ahn & Hogan, 2010), where the stride frequency of humans entrained to an external perturbation over a finite basin of entrainment.

To further study the role of a nonlinear oscillator in walking control, this thesis uses a tool of dynamical systems analysis called a phase resetting curve, which is useful for understanding how a nonlinear oscillator interacts with external perturbations. If a phase resetting curve can be obtained, it serves as a first step in developing a simple model of the oscillator. The focus of this thesis has been to determine if a phase resetting curve can be measured for humans, using an experimental setup where human subjects walked on a treadmill while receiving intermittent ankle torque perturbations. The final result is that no phase resetting was observed, which is not the result expected if a nonlinear oscillator plays a prominent role. However, this result is consistent with the kinematic control of the foot's trajectory, for which there is strong evidence already in the literature.

## Chapter 2 Phase Resetting Curves

This chapter introduces the phase resetting curve, which is a useful tool for studying nonlinear dynamical systems. First, phase resetting curves are described, and second, their use and applications are detailed.

### 2.1 Definition of phase

The phase of an oscillation is simply a unitless variable used to parameterize the oscillation. Over one period, the phase parameterizes the oscillation by time with respect to the period (Ermentrout, 2010). The phase of any instant in time during a period of the oscillation is defined as,

$$\phi(t) = \frac{t-t_k}{t_{k+1}-t_k} \quad \text{Equation 2.1}$$

where the instant in time of interest is  $t$ , the time that the current period began is  $t_k$ , and the time that the current period ends is  $t_{k+1}$ . Thus, the phase increases linearly over the period, where each period begins with  $\phi = 0$  and wraps around to zero again at the start of the next period.

While the choice of the location or feature of the oscillation that corresponds to zero phase is arbitrary in theory, there are some practical considerations in making this choice, discussed in (Pikovsky, Rosenblum, & Kurths, 2001). The zero phase location in the oscillation is defined using the idea of a Poincaré section. Although this thesis does not look at stability analysis of any model or system using a Poincaré Map, a Poincaré section is a useful way to define the zero phase event of human walking.

For an  $n$ -dimensional system, a Poincaré section is an  $n-1$  dimensional surface that is transverse to the flow of all trajectories, such that any trajectories that start on the section flow through it, and not parallel to it (Strogatz, 1994). Also, only crossings in the defined direction are of interest, thus the direction of the trajectory flow through the Poincaré section must be considered. In this thesis, where a walking human is the system of interest, Poincaré sections are approximated using footswitch data, to be described later.

For an autonomous limit cycle process, (Pikovsky, Rosenblum, & Kurths, 2001) note that the phase is a marginally stable variable since  $d\phi/dt$  is constant, which is a direct result from the definition that the phase increases linearly from zero to one over a single period.

Regarding terminology, the terms “phase space” and “phase plane” are not related to the previously defined “phase” of an oscillation. Also, the terms phase lag and phase lead used to describe the phase of a linear system relative to the phase of a forcing function differ from phase “delays” and “advances,” which are described in the next section.

## 2.2 Phase Resetting

A limit cycle's phase may be advanced or delayed by an external perturbation. The following is a description of this concept using a limit cycle in 2-D phase space on the phase plane, shown in Figure 2.1. Also, note that the system dynamics in this description are arbitrary. Zero phase is defined as the Poincaré section where the velocity,  $\dot{x}$ , is held equal to zero, and where we are only interested in Poincaré section crossings from positive to negative velocity (blue line shows Poincaré section crossing).

At phase  $\phi_a$ , a perturbation is applied which displaces the system off the limit cycle (black line), resulting in the perturbed trajectory (red dotted line). The perturbed trajectory settles back to the limit cycle at some further phase indicated by  $\phi_b'$ . The unperturbed trajectory (green line) would have reached phase  $\phi_b$  during the settling interval of the perturbed trajectory. The resulting phase shift for the perturbation applied at  $\phi_p$ ,  $\Delta\phi$ , is then given by the difference in phases at  $b$  and  $b'$ :  $\phi_b' - \phi_b$ . For this perturbation, the system undergoes a phase delay. Using the same convention, a perturbation applied at  $\phi_c$  is shown to result in a phase advance.

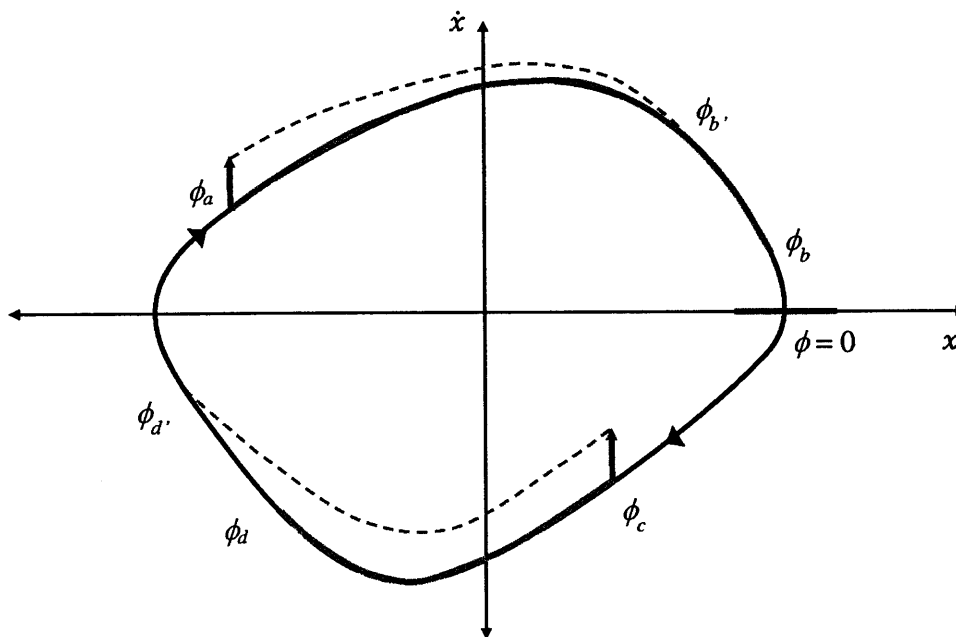


Figure 2.1 Stable limit cycle with two perturbations applied at different phases. The perturbed trajectories (dotted red) settle back to the limit cycle with a different phase when compared to the phase of the respective unperturbed trajectory (green). The perturbation at  $\phi_a$  delays the phase, while the perturbation at  $\phi_c$  advances the phase.

## 2.3 Phase Resetting Curves (PRC)

### 2.3.1 Phase Resetting Curves: Theory and Applications

A phase resetting curve (PRC) plots  $\Delta\phi$  vs.  $\phi_p$ , for all  $\phi_p$  over the period. In general, a PRC is found experimentally by applying perturbations to the system, one at a time, subsequently

measuring the resulting phase shifts. The resulting PRC depends on both the oscillator's dynamics and the shape of the perturbation (Smeal, Ermentrout, & White, 2010).

PRC's are closely related to phase transition curves, or PTC, which were first introduced by Arthur Winfree for the purpose of studying biological clocks and circadian rhythms (Winfree, 2001). A PRC contains the same information as a PTC, but plotted differently. On a PTC, the vertical axis shows the final phase after a perturbation, not the phase shift. As with other terms in nonlinear dynamics that are still in flux, PRC's are sometimes called PTC's and vice versa; this thesis follows the terminology used in experimental neuroscience.

For limit cycle oscillators that are asymptotically stable, there are several theoretical results that build upon PRC's that provide highly useful insight into the oscillator's behavior. From a single state of an asymptotically stable oscillator, a PRC using a weak perturbation can be determined by numerical or experimental methods. This "infinitesimal" PRC, allows for the construction a phase model that can be used to predict the oscillator's entrainment behavior in response to an external periodic perturbation (Galan, Ermentrout, & Urban, 2005). For example, predictions can be made for the specific phases at which the oscillator will phase-lock to the perturbation. Further, the phase model can be used to predict synchronization behavior in coupled oscillator networks, which are a central topic in understanding neural processes (Smeal, Ermentrout, & White, 2010).

### **2.3.2 Computation of Experimental PRC's**

Except for perhaps the rarest examples, PRC's must be computed numerically or computed from experimental data. As an alternative illustration of phase resetting, consider the oscillator plotted in time in Figure 2.2. This description will also detail simple computations for finding PRC's from data. The dynamics in this 2-D example are arbitrary, and are not intended to match the previous example in Section 2.2.

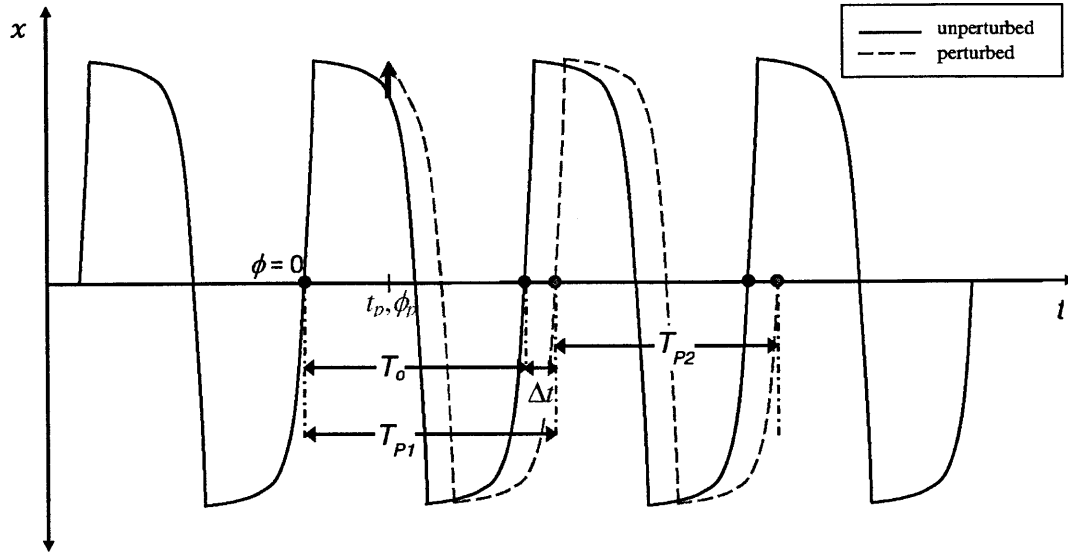


Figure 2.2 Limit cycle oscillator waveform plotted in time. The perturbation causes the perturbed trajectory to be delayed (negative phase shift), and the phase shifts are computed using the  $\Delta t$  between the Poincaré section crossings.

The unperturbed limit cycle oscillator (black line) with intrinsic period  $T_0$  is plotted in time, with zero phase (black dots) defined by the Poincaré section,  $x = 0$ , with crossing direction from negative to positive  $x$  (note Poincaré sections exist in phase space, not plots in time). At time  $t_p$  (phase,  $\phi_p$ ), a perturbation is applied, resulting in the perturbed trajectory (dotted red line). The perturbed trajectory reaches the Poincaré section (red dot) after period  $T_{P1}$ . If the assumption can be made that the oscillator settles back to the limit cycle by the end of  $T_{P1}$ , then the phase shift is computed as

$$\Delta \phi = \frac{\Delta t}{T_0} = \frac{T_0 - T_{P1}}{T_0}. \quad \text{Equation 2.2}$$

After  $T_{P1}$ , the oscillator continues with period  $T_0$  ( $T_{P2} = T_0$ ). By repeatedly applying perturbations at a sufficiently fine distribution of  $\phi_p$ 's throughout the limit cycle, and allowing settling to occur, the phase resetting curve can then be plotted. If the assumption of same-period settling is violated, where  $T_{P2} \neq T_0$ , then additional periods must be included in computing  $\Delta t$ . If the system settles during  $T_{P2}$ , then the phase shift is computed as

$$\Delta \phi = \frac{\Delta t}{T_0} = \frac{2T_0 - (T_{P1} + T_{P2})}{T_0}. \quad \text{Equation 2.3}$$

For systems that do not settle in  $T_{P1}$ , the theory referenced above cannot be used without some modification. In experiments that do require  $T_{P2}$  for settling, the PRC theory has been successfully modified to yield useful predictions about synchronization (Oprisan, Prinz, & Canavier, 2004). Also, Oprisan suggests that beyond 2 periods “the bookkeeping becomes intractable.” While not stated explicitly, this is likely due to variability of the system’s period,

which may confound the computation of phase resetting. However, if the magnitude of the phase shift is large relative to the period variability, then looking beyond period  $T_{P2}$  may allow for phase resetting to be estimated (Feldman, Krasovksy, Banina, Lamontagne, & Levin, 2010), (Nomura, Kobayashi, & Kozuka, 1998).

## Chapter 3 Experimental PRC of Human Walking

This chapter describes the experiments conducted to measure a PRC for unimpaired human walking using a torque perturbation at the ankle. The following sections describe the experimental setup, protocol, data analysis, and results.

### 3.1 Subjects

Nine male subjects were recruited on the basis of being acquaintances of the investigator. Subjects were included on the basis of having no reported history of neural abnormality. All subjects gave informed consent after receiving an explanation of the experiment. Table 3.1 shows the age, height, weight and chosen walking speed (defined below) for the 9 subjects.

	Mean $\pm$ std. dev.	Range
Age (yrs.)	25 $\pm$ 2.7	22 – 31
Height (ft., in.)	5' 11" $\pm$ 2.8	5'8" – 6'5"
Weight (lbs.)	165 $\pm$ 19	135 – 195
PWS (mph)	2.3 $\pm$ 0.41	1.7 – 3.0

Table 3.1 Mean and standard deviation of physical characteristics and PWS (defined below) of experiment subjects.

### 3.2 Experimental Setup

#### Perturbation Device

A robot called the Anklebot was used to apply the plantarflexion perturbations during the PRC experiments. The Anklebot is a novel, 2 DOF device that can be used to apply torques about two axes. For a full characterization of the Anklebot, see (Roy, et al., 2009). The Anklebot is controlled via a Tcl/Tk script running inside a real time Linux kernel. The system computer collects Anklebot data such as torque commands and ankle position, as well as other sensors described below, all at a sampling rate of 200 Hz.

The perturbation applied by the Anklebot was a 140ms torque pulse which acted to plantarflex the ankle, which is the motion undergone when pointing one's toes. The main muscles that actuate plantarflexion are the soleus and gastrocnemius. The magnitude of the perturbation was 6 Nm when the shank was at a right angle to the sole of the foot. While the magnitude of the force applied by the Anklebot was constant, the applied torque varied because the moment arm varied slightly due to the angular travel of the ankle during walking. The minimum moment arm will occur at maximum deflection, which occurs during maximum ankle plantarflexion, which is on average about 20° (Perry, 1992). Thus the actual torque applied was in the range of 5.6 – 6 Nm.

The magnitude was chosen to be as large as possible while still remaining within the comfort range of all subjects. This was determined through several iterations of the experimental protocol. Subjects reported that the discomfort induced by perturbations occurred during swing phase, most notably when perturbations occurred just before heel strike. The interruption of heel strike elicited a surprising sensation and may have evoked a startle response. This effect was not studied in this thesis, though it may provide interesting information about the feedback used by the neural controller. The chosen magnitude was relatively light and easy to walk with, and as a result, any phase shifts were expected to be small in magnitude.

### **Donning Experimental Hardware**

The experimental session began with fitting and attaching the hardware and sensors to the subject's dominant leg, determined by kicking preference. First, two footswitches used to detect toe-off and heel strike were taped to the bottom of the bare foot on the big toe and the heel. A footswitch is a variable resistor that decreases in resistance when pressure is applied. The sock was then put on, and a custom shoe with a mounting bracket for the Anklebot was put on the foot. Then, an appropriately sized knee brace, also with mounting bracket for the Anklebot, was attached to knee. The knee brace has a potentiometer for measuring the angle of the knee.

All knee brace straps were tightened firmly to reduce brace sliding but not to an extent to cause discomfort. In particular, the strap around the upper part of the gastrocnemius was re-tightened as the final fitting step to ensure support for the weight of the Anklebot. After fitting the knee brace, the subject was instructed to swing the knee several times to assess proper joint alignment and general comfort.

Next, a shoulder strap was attached to a loop on the knee brace and run up around the neck as another means to prevent the brace from sliding. Lastly, the Anklebot was mounted to the knee brace and shoe mounting brackets.



Figure 3.1 Experimental setup. Subject on treadmill wearing the Anklebot with custom shoe and knee brace.

### Zeroing the knee brace

## 3.3 Experimental Protocol

### 3.3.1 Warm-up: Finding the Preferred Walking Speed and Perturbation Demonstration

The first task during warm-up was to zero the knee brace. The subject was instructed to stand with their weight shifted to the non-dominant side, and subsequently asked to rest the dominant heel in front of their body so that the knee was fully extended against the limit of the knee brace, if the limit could even be reached. This follows the convention that that a fully extended knee (straight leg) has an angle equal to zero. A demonstration was provided by the investigator.

Next, the subject was guided through a walking warm up that lasted approximately 10 minutes. The purpose of this warm up was to allow the subjects to choose a preferred walking speed (PWS) on the treadmill and to experience a demonstration of the perturbations.

The preferred walking speed was the treadmill speed that the subjects chose to walk for the duration of the experiment. The purpose of finding a preferred walking speed was twofold.

First, there is some evidence that there is an over ground walking speed that is preferred by the neural controller. Evidence of such a preference appears as a reduction in hip flexor activity during swing phase in some subjects studied, to the extent of zero hip flexor activity (Perry,

1992). One hypothesis to account for this observation is that the neural controller takes advantage of the pendular dynamics of the leg in swing phase. Since settling to the nominal walking limit cycle is imperative to obtain a PRC, the PWS selection process was done to accommodate this possible neural preference.

The second purpose, which may be related to the first with regard to efficiency, is to ensure that the subjects become accustomed to the Anklebot and comfortable with its added mass. Further, letting the subject choose the speed at which they can comfortably walk for 20 minutes minimizes fatigue.

The instructions below were verbally provided by the investigator to guide the selection of the PWS. Subjects were repeatedly reminded that natural, comfortable walking was the primary objective. To reinforce this objective, the treadmill's speed display was covered. The subjects alone controlled the speed of the treadmill using buttons on the handrails, which ensured that they accelerated at their own rate and were not influenced by the investigator.

1. Choose a speed that feels natural and comfortable. [Hold for approximately 1 minute]
2. Increase the speed of the treadmill by several ticks until you feel it is too fast to walk comfortably for 20 minutes [Hold approximately 30 seconds at "Fast" speed]
3. Decrease the speed back to a comfortable, natural speed [Hold approximately 30 seconds at "Comfortable" speed]
4. Decrease the speed by several ticks until you feel it is too slow to walk naturally [Hold approximately 30 seconds at "Slow" speed]
5. Increase the speed back to a comfortable, natural speed [Hold approximately 30 seconds at "Comfortable" speed]
6. Repeat Steps 1-5
7. Use the final 2<sup>nd</sup> round "Comfortable" speed as the PWS

Subjects then stood still on the treadmill for a 2 minute break while the software was started. A perturbation demonstration was provided, first with the treadmill stopped, and second with subject walking at the PWS. About 20 perturbations were applied while walking to ensure subject's familiarity with the setup and also to estimate the subject's stride period,  $T_{est}$ , which was entered in software to control perturbation timing.

### **3.3.2 Data Collection: Walking with Perturbations**

Next, the data collection portion of the experiment began. Subjects were again instructed to walk comfortably and naturally. The data collection portion of the experiment was separated into three stages. Stage 1 consisted of 90 seconds of unperturbed walking, Stage 2 consisted of about 20 minutes of walking with 400 pseudo-randomly timed perturbations, and Stage 3 consisted of another 90 seconds of unperturbed walking. The perturbation control scheme, detailed below, was designed to apply 400 perturbations uniformly distributed over the stride period. The phases at which the perturbations were applied were pseudo-randomly ordered to prevent entrainment,

which was shown to occur for a periodic perturbation with a period within the basin of entrainment (Ahn & Hogan, 2010). Each subject received the same order of perturbations.

The perturbations during Stage 2 were controlled via the system computer running a Tcl/Tk script. The script monitored positive crossings of a threshold knee angle (knee brace potentiometer voltage) to detect the onset of the large flexion peak during swing phase. After this event, a perturbation was applied after a time delay equal to some fraction of  $T_{est}$ . In this manner, using a uniform distribution of time delays ranging from zero to  $T_{est}$ , the 400 perturbations were distributed approximately uniformly over the stride period. After each perturbation, the computer stopped monitoring the knee angle for  $1.5T_{est}$ , which ensured that no perturbations will occur during the next stride period,  $T_{P2}$ . This pause was introduced because pilot studies indicated that the response to perturbations of the magnitude delivered sometimes required more than one stride but settled within two strides or less.

The number of perturbations chosen was based on (Galan, Ermentrout, & Urban, 2005), which showed that for perturbations that produce small phase shifts buried in inevitable noise, a large number of data points is needed so that regression can recover the true shape of the PRC.

### **3.4 Data Analysis**

This section details the data analysis, which was done using MATLAB v7.12 (The Mathworks, Natick MA). The data used in the analysis included the knee brace angle, Anklebot torque commands, and toe and heel switch voltages.

#### **3.4.1 Knee Brace Angle: Zeroing and Filtering**

As described in the experimental protocol, the zero knee angle for each subject was found by asking subjects to fully extend the knee brace. When in this position, the knee angle was sampled for 2 seconds (2000 ms), and subsequently averaged to provide a zero value for the knee angle.

The knee angle was used to observe the limit cycle behavior of the subjects when walking. This entailed finding the angular velocity, thus filtering was needed to remove noise before differentiating. The knee angle was filtered forwards and backwards using a low pass FIR filter with cut off frequency of 7.5 Hz to remove noise. No other filtering of data was needed.

#### **3.4.2 Footswitch Event and Poincaré Section Identification**

Before doing any phase resetting computations, a Poincaré section was chosen. In general, any periodic, identifiable event could be used, however, since the perturbations from the Anklebot affected the stride kinematics, a Poincaré section had to be chosen that could be identified reliably in the presence of perturbations. For example, the heel switch voltage was used to detect heel strike, but perturbations just prior to heel strike were found to plantarflex the ankle and raise the heel, thus delaying the heel strike. Whether this delay resulted in phase resetting was unknown initially, and alternatives were considered. The final choice, for all subjects, was toe off

because perturbations had no observable effect on this event, likely due to the configuration of the leg at toe off and the constraint of contact with the ground before toe off.

The method for identifying toe off in the analysis code is described here, and an example result is shown in Figure 3.2. First, a suitable threshold value for toe off was chosen. Second, the signal indices of all falling edges that crossed the threshold value were identified. Since the edges have short times scales, there are relatively few samples per edge. Therefore, when detecting a falling edge threshold crossing, the identified signal sample may appear below the threshold. Finally, starting at the first of these indices, all subsequent indices were “scanned” for false events by ensuring that the  $n+1^{\text{th}}$  index was separated in time from the  $n^{\text{th}}$  index by a chosen time buffer,  $t_{\text{buffer}}$ , which ranged from 0.5 to 1 second depending on the event being identified. This final scanning step was critical for proper identification of some subjects’ toe off events (and other events as well), which filtered out many small noise edges that caused false event identifications, as well as perturbation effects, and spurious toe movement.

The methods for identifying the other events shown in Figure 3.2 were nearly identical except for the values of the algorithm parameters. These parameters were “tuned” for each subject as the footswitch signal waveform varied greatly in appearance across the nine subjects. The effects of the shoe’s fit and perturbations also seemed to vary, though this was not studied.

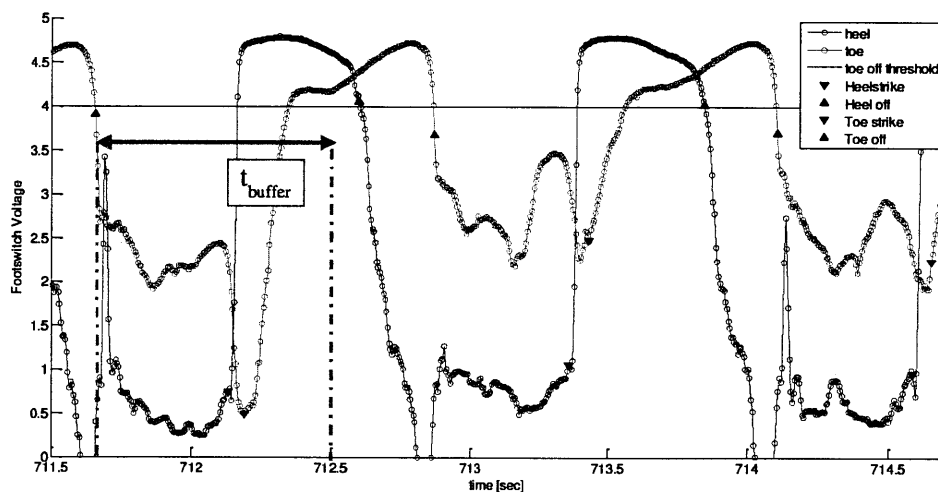


Figure 3.2 Example footswitch data with markers of four events: heel strike, heel off, toe strike, and toe off.

For two of the nine subjects, the toe switch failed during the experiment. Fortunately, the heel switch signal contained a feature informally called “heel slap,” which occurred every stride in these two subjects (data from several other subjects also had this feature). This event is caused by the heel of the shoe striking the heel of the foot at some instant near toe off, similar to the behavior of a “flip-flop” sandal. The validity of this event as a substitute for toe off is evident in Figure 3.2 above, where the sharp edge in the heel switch data coincides exactly with the falling edge of the toe switch. Figure 3.3 below shows an

example from one of the two subjects in which the toe switch failed. The heel slap event yielded a stride period standard deviation that was very similar to values obtained from other subjects computed using toe off, shown in Table 3.2. The algorithm for identifying heel slap was similar to that for toe off, except that a rising edge threshold was set so that the signal crossed at a time shortly after the onset of the actual edge. This was necessary to avoid detecting non-heel slap edges that occurred in swing phase. To gain a better edge estimation in time, the index of heel slap was stepped backward to the previous index to produce a better measure of the edge in time. This places the marker below the threshold.

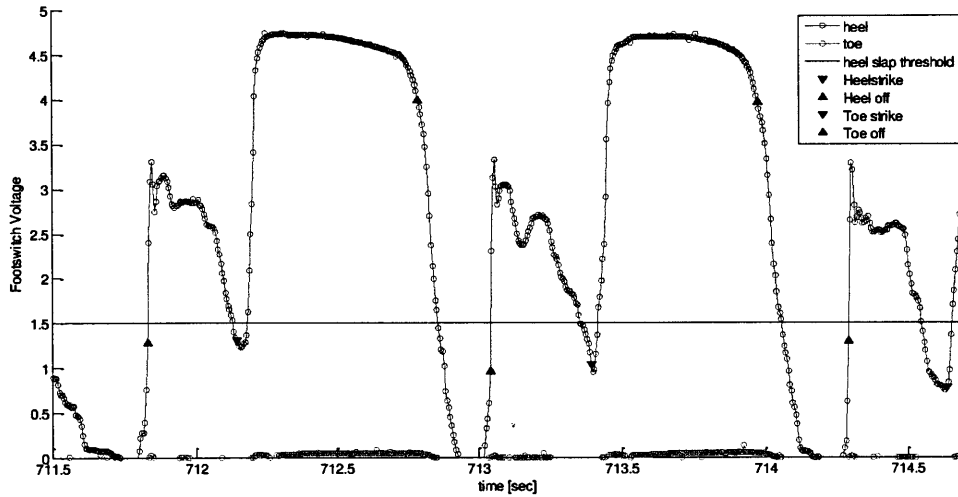


Figure 3.3 Footswitch data showing heel slap event used as a substitute for toe off. A toe off marker is shown at the heel slap events.

Subject	All strides, mean $\pm$ std. dev.
1	1.308 $\pm$ 0.022
2	1.201 $\pm$ 0.024
3	1.404 $\pm$ 0.032
4	1.316 $\pm$ 0.025
5	1.219 $\pm$ 0.020
6 (heel slap)	1.273 $\pm$ 0.036
7	1.312 $\pm$ 0.030
8	1.257 $\pm$ 0.028
9 (heel slap)	1.392 $\pm$ 0.031

**Table 3.2 The mean and standard deviation for all subjects' stride periods, showing the close agreement in stride period standard deviation of toe off vs. heel slap.**

### **3.4.3 Computing and Classifying the Stride Periods,**

Each stride period is simply the difference in time between adjacent Poincaré sections.

All strides during Stage 2, walking with perturbations, were classified into one of three “types,” which will simplify communication of the analysis performed. The stride during which a perturbation is applied is called a “Period-1” stride, and the immediately following stride is called a “Period-2” stride, so that there were 400 of each type of stride. Lastly, the third and final classification of strides is a Period-3 stride; these strides follow Period-2 strides. They were located in software by looking for unperturbed strides that occurred after Period-2 strides.

There were approximately 200 Period-3 strides for each subject. The variation of this number arose because a Period-3 stride only occurred after a perturbation late in a stride, where the  $1.5T_{est}$  pause lasted until about halfway into the Period-3 stride. After this pause, if the knee angle had already passed the rising edge trigger threshold, no perturbation was triggered for this Period-3 stride.

### **3.4.4 Computing the Intrinsic Stride Period and Verifying it is Constant**

Before computing phase resetting, the intrinsic stride period was found. To do so, all stride periods were plotted vs. stride number. In Figure 3.4, the Stage 1 and 3 stride periods show a similar distribution to the Stage 2 stride periods. However, this is not the case in Figure 3.5, where there is a visible difference in distributions between Stages. While statistical tests could be performed to verify that Stages 1 and 3 differ from 2, it was deemed unnecessary as the Period-3 strides provided a more meaningful measure of the Stage 2 intrinsic period since they are unperturbed and fully settled; the fact that Period-3 strides have settled will be shown below. The best measure of the intrinsic period,  $T_0$ , was computed by averaging all Period-3 strides. Lastly, it is important for the phase resetting computations to verify that the intrinsic period does not change throughout the perturbed walking in Stage 2. This was verified for all subjects as the Period-3 strides, and even all strides in Stage 2, show no significant deviation about the dotted  $T_0$  line. Papers from experimental neuroscience literature report that the intrinsic period of a neuron may show variability up to 10%, and still allow for a valid PRC to be estimated (Oprisan, Prinz, & Canavier, 2004). Although it is not stated whether 10% refers to the range (max, min) of the variability or the standard deviation, in the Results section below it is shown that the standard deviation of the walking intrinsic period was on the order of 3-4%; well within either possible interpretation of the limit.

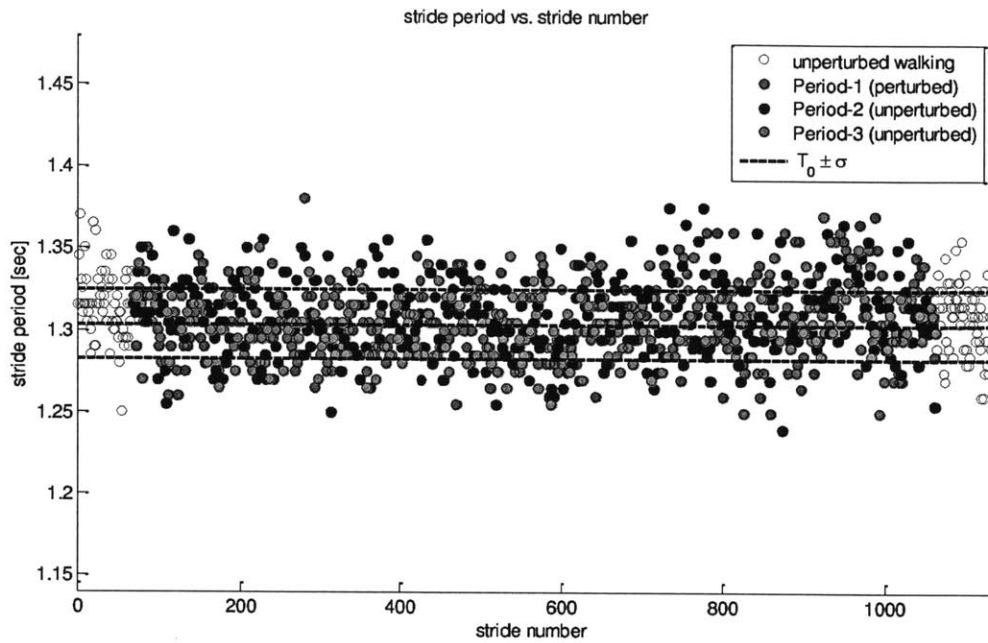


Figure 3.4 All stride periods for Subject 1, showing that the Stage 1 and 3 stride periods have a very similar distribution to that of Stage 2.

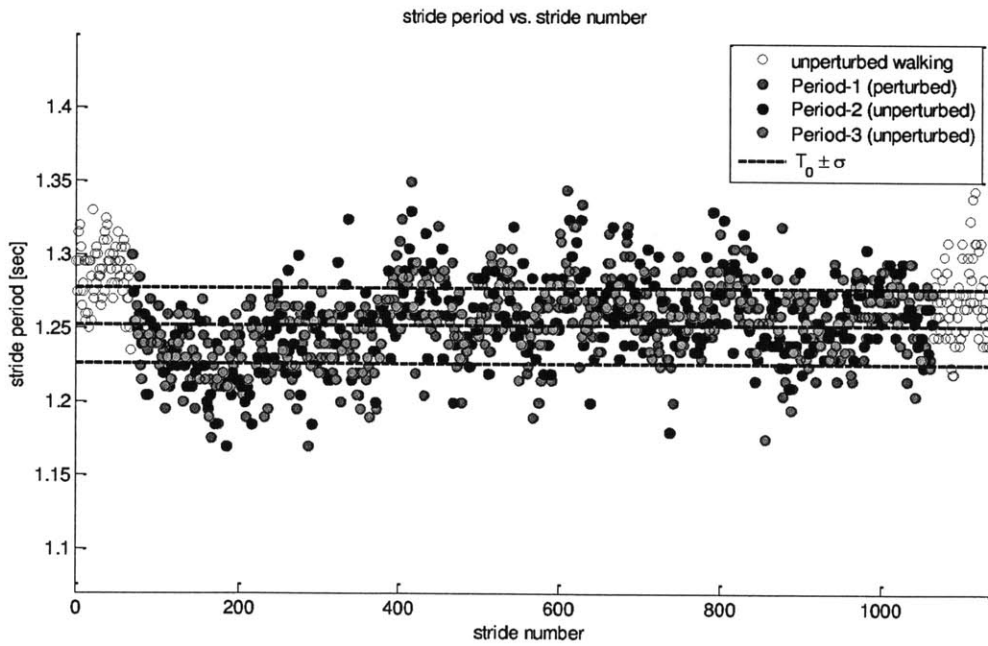


Figure 3.5 All stride periods for Subject 8, which indicate that Stages 1 and 3 have different distributions than Stage 2, and thus Stages 1 and 3 are not usable for computing the intrinsic stride period.

### 3.4.5 Verifying stride settling within two strides

Another important component of the phase resetting computation was to verify that the perturbed trajectories settled back to the nominal limit cycle within two strides. To study stride settling, the knee brace angle was plotted against its angular velocity, which results in a 2-D “knee plane” plot that shows the limit cycle behavior of human walking. Although human walking dynamics may have system order far greater than two, this knee plane plot served as a useful way to assess stride settling.

To verify that a perturbed stride had settled, the limit cycle behavior of the unperturbed gait was established, along with an appropriate “settled band,” within which trajectories were assumed fully settled. As discussed in the previous section, the Period-3 strides provide the best estimate of the intrinsic period during perturbed walking. In Figure 3.6 and Figure 3.7, the Period-3 strides are plotted in blue, showing a highly repeatable trajectory with apparently low variability, or width. To verify that this variability is characteristic of unperturbed, fully settled stride kinematics, it was compared to the Stage 1 strides also plotted in the knee plane. The Period-3 trajectory showed only slightly greater variability throughout the majority of the stride. Some subjects, such as Subject 1 in Figure 3.6, showed greater variability and a shift in the smaller flexion circle which occurs during the stance phase. Nevertheless, the repeatability of the behavior still indicates the trajectory is not in transient settling or otherwise perturbed. Subject 8’s plot shows excellent consistency in the Period-3 trajectory, even when compared to the Stage 1 trajectory. These plots show that the Period-3 strides exhibited repeatable limit-cycle behavior. They were used to establish a “settled band” to determine whether perturbed strides during stage 2 settled before the end of Period-2.

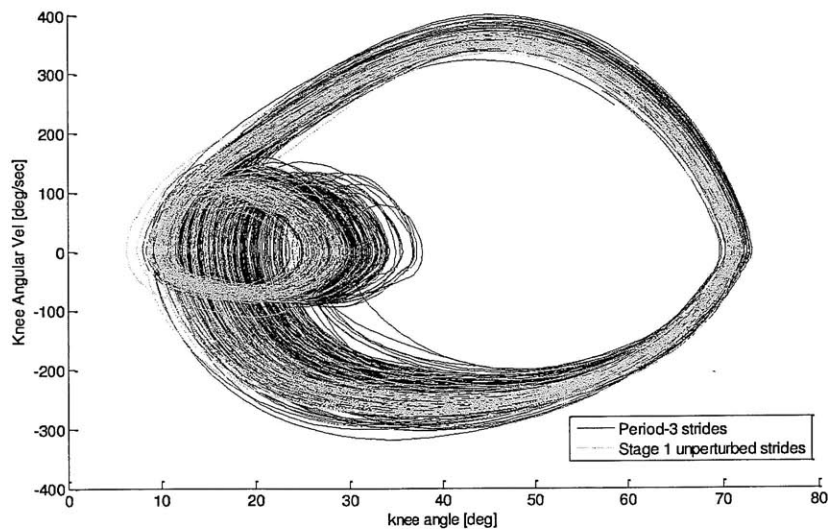


Figure 3.6 Period-3 strides and Stage 1 unperturbed strides plotted in the knee plane for Subject 1. The Period-3 band of trajectories shows only slightly greater variability and was used as a valid representation of the limit cycle behavior.

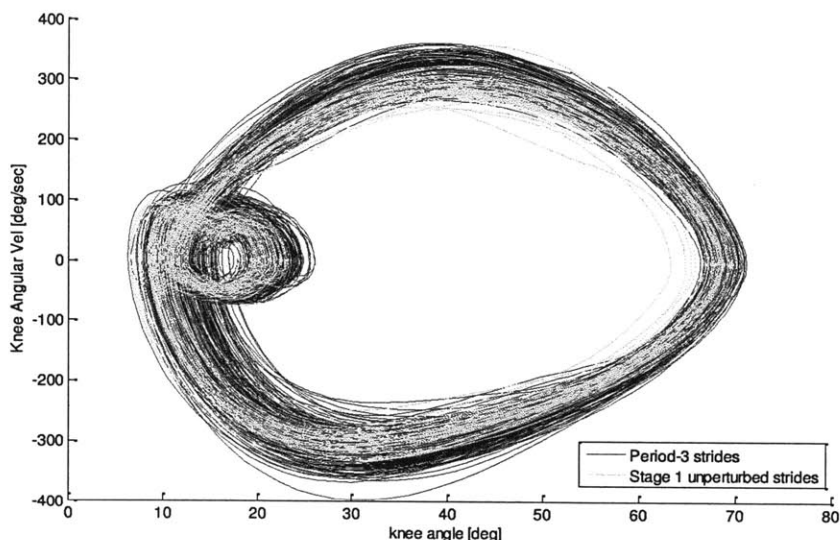


Figure 3.7 Period-3 knee plane plot and Stage1 unperturbed knee plane plot for Subject 8.

Finally, the perturbed strides were plotted over the Period-3 “settled band” to ensure that at the conclusion of the Period-2 stride, the trajectory was within this band. To facilitate this visual inspection, all Period-1 strides and the associated Period-2 strides were sorted by the phase of the applied perturbation. The phase of the perturbation was computed as

$$\phi_p = \frac{t_p - t_{P1}}{T_0}, \quad \text{Equation 3.1}$$

where  $t_p$  is the instant of perturbation onset,  $t_{P1}$  is the instant of the previous Poincaré section crossing prior to  $t_p$ , and  $T_0$  is the intrinsic period as computed above. After sorting the Period-1 strides by perturbation phase into ten phase bins with width 0.1, the Period-1 trajectories and the following Period-2 strides in each bin were plotted. Two example plots are shown in Figure 3.8 and Figure 3.9. As shown in the legend, each Period-1 stride is a red line that begins with a green marker at the Poincaré section (toe off) and moves clockwise around the plot. At some phase during the stride, a perturbation was applied. At the next crossing of the Poincaré section, the trajectory changes color to black for the Period-2 stride, and continues to the Poincaré section, where it ends at a red dot. The location of these red dots within the settled band is clear evidence that settling has occurred during the Period-2 strides. If settling did not occur, these red dots would be located outside of the settling band.

During data analysis, the 10 plots for each subject were inspected for settling.

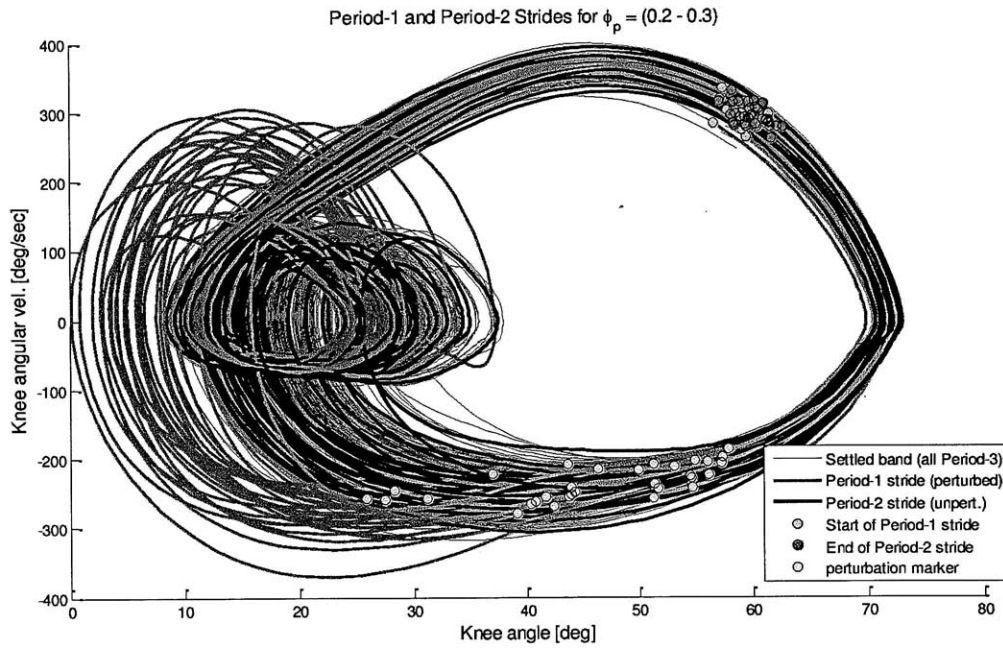


**Figure 3.8** Knee plane plot showing Period-1 trajectories perturbed at phases between 0.2 – 0.3, and the following Period-2 trajectories. Note that all red dots lie inside the settled band (blue), which is clear evidence that all Period-2 trajectories had settled. (Subject 1)

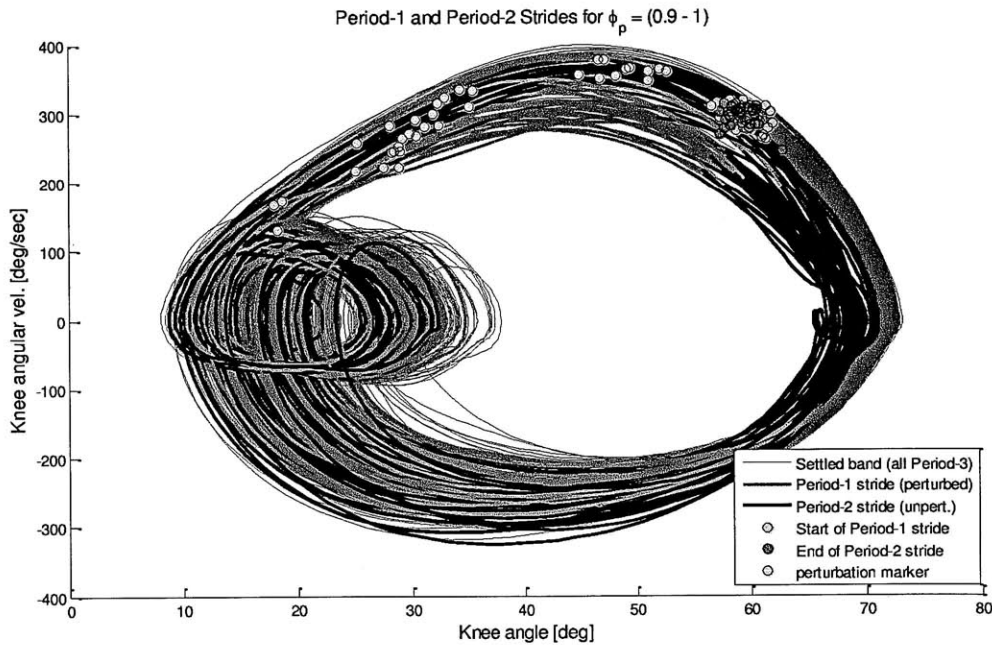


**Figure 3.9** Knee plane plot showing Period-1 trajectories perturbed between phases 0.9 – 1. All Period-2 strides have settled as all red dots lie inside the settled band. (Subject 1)

### Verifying uniform phase distribution

To ensure the perturbation control software successfully distributed the 400 perturbations uniformly throughout the stride, histograms were plotted showing the number of perturbations applied in each of ten phase bins. The data for two subjects below show sufficiently uniform distributions, with the remaining subjects showing uniformity similar to these, or better.

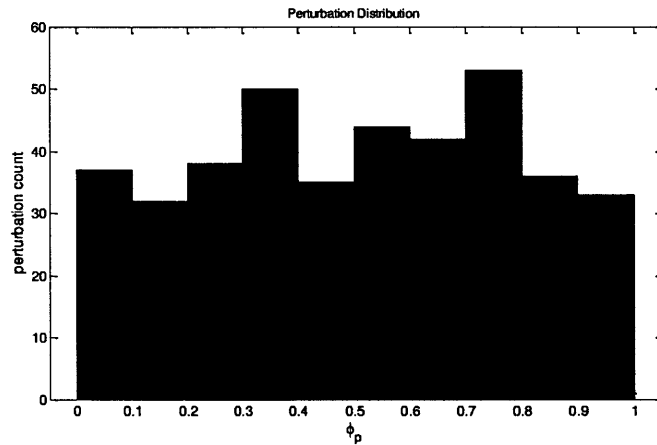


Figure 3.10 Perturbation phase distribution for Subject 5.

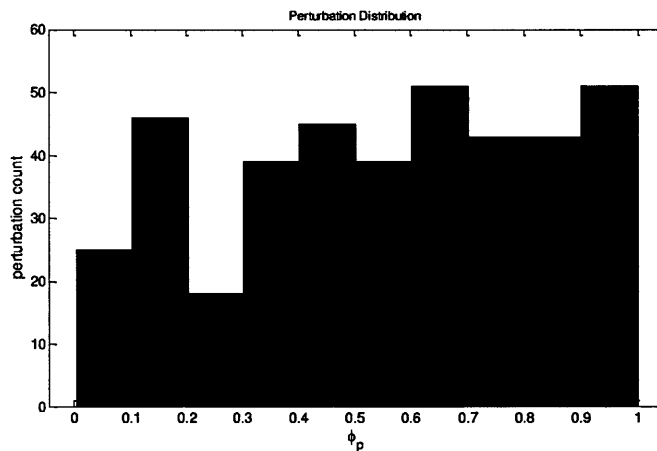


Figure 3.11 Perturbation phase distribution for Subject 6.

### 3.4.6 Computing the phase shift

After the intrinsic period was found, verified sufficiently constant and all perturbed trajectories were shown to settle during Period-2, the phase shifts were computed using Equation 2.3 from Section 2.3.2.

### 3.4.7 Plotting the PRC and a Least Squares Fourier regression

With the phase shifts and perturbation phases computed, the PRC was then plotted. However, as is commonly seen in the literature, simply plotting of the PRC points may not reveal the shape of

the PRC due to unavoidable variability. Since the experimental measurements may have added noise and variability appears to be an intrinsic property of the underlying behavior, this experimental method relied on a large number of data points and subsequent regression to uncover the shape of the PRC. A regression model for the PRC points was chosen, and analysis was done on the regression to determine if it explained a sufficient amount of variation in the data.

The chosen regression was a least squared error fit to a Fourier series model. A Fourier series is a logical and straightforward choice since PRC's are periodic, a fact due the phase wrap-around at 1. The regression equation was

$$\Delta \hat{\phi} = a_0 + \sum_{n=1}^h a_n \cos(n \cdot 2\pi\phi_p) + b_n \sin(n \cdot 2\pi\phi_p), \text{ Equation 3.2}$$

where the  $h$  index denotes the number of harmonics used in the fit.

### 3.5 Results

The top panel in Figure 3.12 shows the PRC data plotted along with Fourier regression with 10 harmonics. Fewer harmonics were tried initially, but the  $R^2$ , which is a measure of the data variance accounted for by the regression, was extremely low. The  $R^2$  value for  $h = 10$  for this subject is 0.08, very low, and increasing the number of harmonics further brought little improvement in  $R^2$ . The residuals for  $h = 10$  are plotted in Figure 3.13 and contain no pattern with approximately zero mean, which indicates further increasing  $h$  would do little to improve the regression fit.

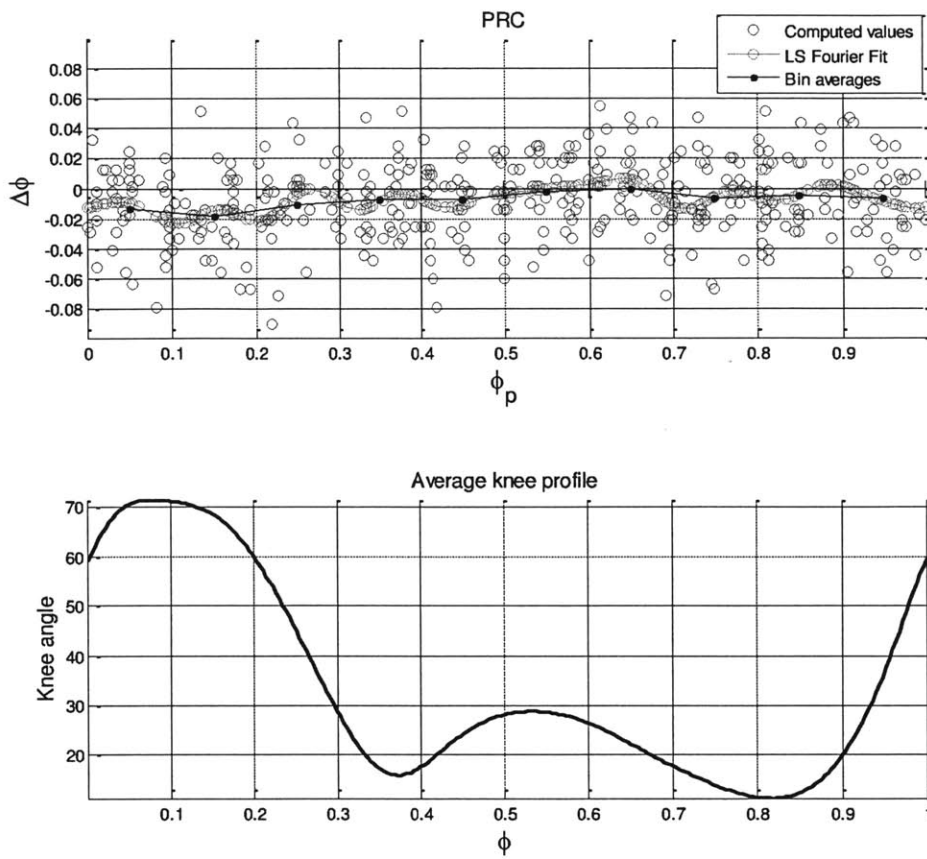


**Figure 3.12** The top panel shows the PRC obtained from a least squared error regression to a Fourier series model with ( $h=10$ ). The bottom panel shows an averaged knee profile for the subject, to provide a reference for the configuration of the leg. (Subject 1)

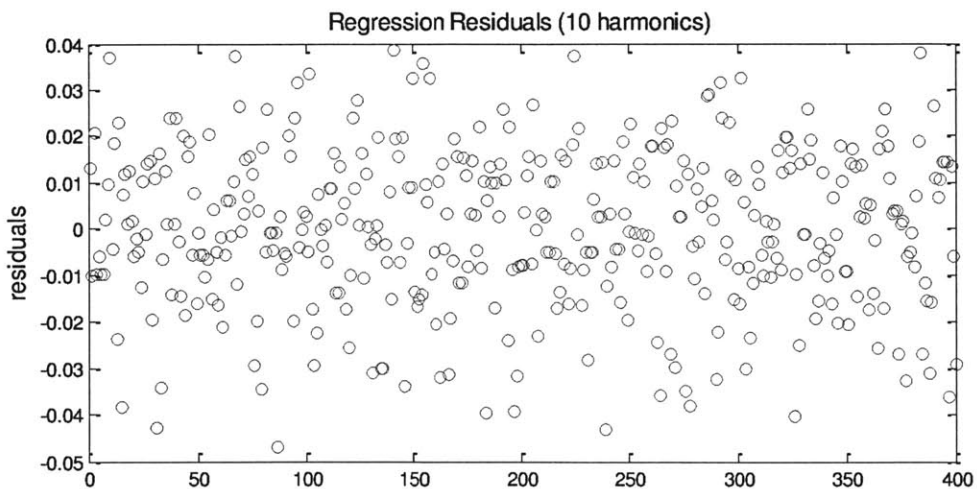


**Figure 3.13** Residuals for the regression fit for Subject 1 above. The absence of pattern in the residuals indicate that increasing the number of Fourier coefficients by increasing  $h$  will not improve the fit.

The PRC results for all 9 subjects are presented here, along with several statistics. All plots used in the analysis for all subjects are contained in Appendix A: Stride Periods Plots.

There were no adverse events to report aside from the failure of the toe switches, as described in Section 3.4.2. One subject asked to wear the Anklebot on the non-dominant side because his dominant knee almost fully recovered from a prior injury. The Anklebot was worn on his non-dominant side, and when asked during the experiment about knee pain, the subject reported no discomfort.

Table 3.3 shows the mean and standard deviation of the Period-3 strides used to compute  $T_0$ , well as all strides from all three Stages.

Subject	$T_0$ (Period-3 mean) $\pm$ std. dev.	All strides, mean $\pm$ std. dev.
1	1.303 $\pm$ 0.021	1.308 $\pm$ 0.022
2	1.200 $\pm$ 0.022	1.201 $\pm$ 0.024
3	1.405 $\pm$ 0.030	1.404 $\pm$ 0.032
4	1.314 $\pm$ 0.023	1.316 $\pm$ 0.025
5	1.218 $\pm$ 0.017	1.219 $\pm$ 0.020
6 (heel slap)	1.270 $\pm$ 0.035	1.273 $\pm$ 0.036
7	1.308 $\pm$ 0.030	1.312 $\pm$ 0.030
8	1.252 $\pm$ 0.026	1.257 $\pm$ 0.028
9 (heel slap)	1.390 $\pm$ 0.027	1.392 $\pm$ 0.031

**Table 3.3 The mean and standard deviation for the intrinsic period  $T_0$  and "All Strides"**

The PRC's from each subject are shown in Figure 3.14 through Figure 3.18. Also plotted with the PRC points are the Fourier regression and the average phase shift in each phase bin. The  $R^2$  value for each regression is shown in the figure caption. The averaged knee profile during the stride is plotted in the bottom panel for referencing the leg configuration.

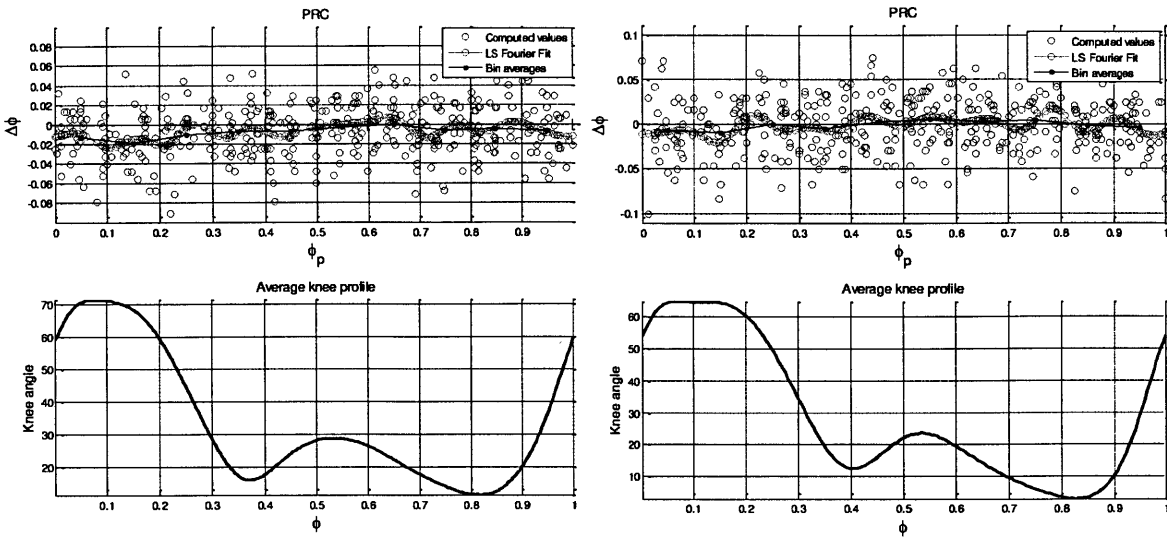


Figure 3.14 PRC's: Subject 1,  $R^2 = 0.07$  (left) and Subject 2,  $R^2 = 0.07$  (right)

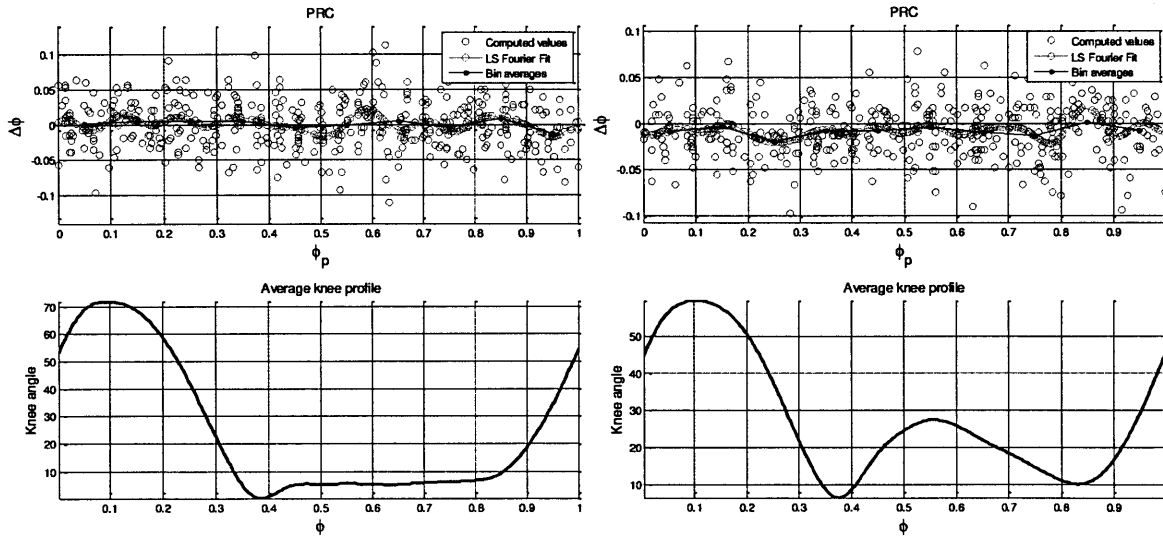


Figure 3.15 PRC's: Subject 3,  $R^2 = 0.06$  (left) and Subject 4,  $R^2 = 0.06$  (right)

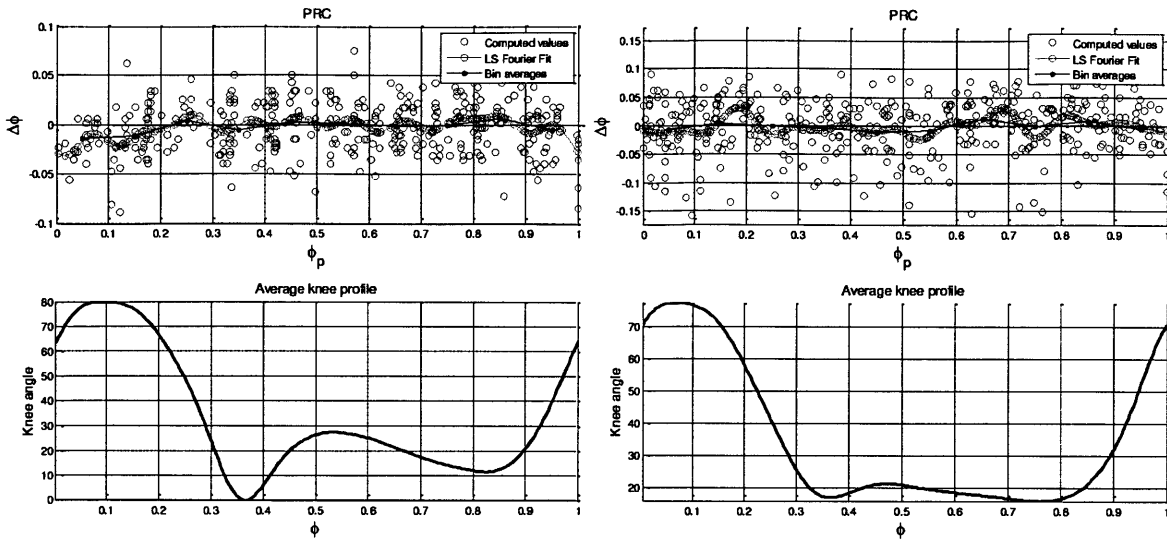


Figure 3.16 PRC's: Subject 5,  $R^2 = 0.10$  (left) and Subject 6,  $R^2 = 0.07$  (right)

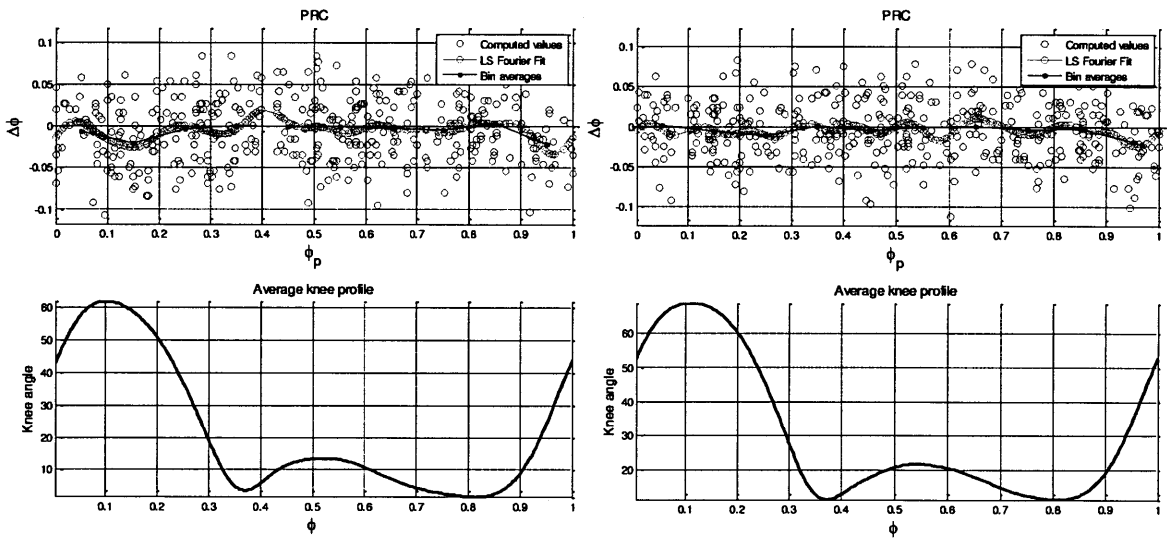


Figure 3.17 PRC's: Subject 7,  $R^2 = 0.06$  (left) and Subject 8,  $R^2 = 0.04$  (right)

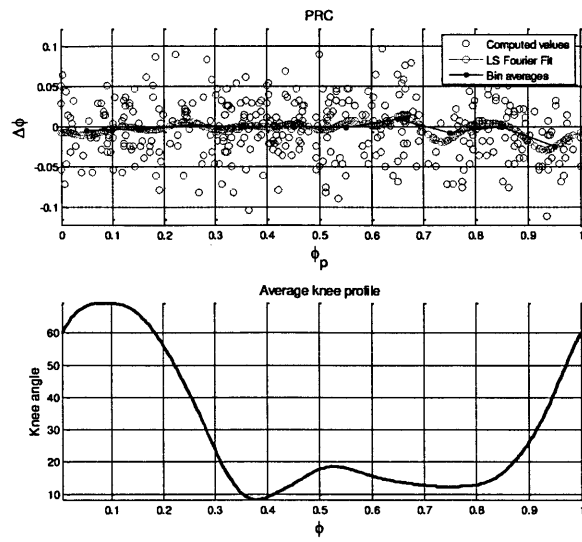


Figure 3.18 PRC: Subject 9,  $R^2 = 0.05$

## Chapter 4 Discussion and Conclusions

### 4.1 PRC's for all Subjects were Indistinguishable from Zero

The Fourier regression for each subject has a very low  $R^2$  value, which shows that the regression barely accounts for the observed variance in the observations of phase resetting. The inescapable conclusion for this experiment is that the PRC is zero. The Fourier series is an ideal choice for fitting a PRC due to its periodicity, so there is no reason to pursue other regression models. Additionally, the plot of residuals for each subject's PRC regression showed no pattern with approximately zero mean, indicating that the number of coefficients in the regression is sufficient. Finally, there was no consistent pattern among the subjects.

### 4.2 Considering the Potential for Artifact in the Zero PRC's

Before interpreting the implications of a zero PRC, the possibility of an inaccurate PRC is considered here. It is possible that phase resetting may have occurred, but it was not detected by the analysis method used. However, the method used is very similar to that of other studies that have successfully measured PRC's for endogenously bursting neurons. Although a neuron is a drastically different system, both human walking and neurons are capably modeled by limit cycle oscillators which means the methods of analysis will be necessarily similar.

In other studies, the collection of a large number of PRC points has ensured enough information is contained in the data to uncover the PRC from noise. The PRC experiments here used exactly that approach, and still did not find any meaningful regression from the data. Although there is no reason to suspect excessive noise in this study, one improvement to the analysis that might reduce noise would be to measure phase resetting using a mixed pair of Poincaré sections, so that the total time elapsed is shorter than two full strides. This would require studying the settling plots and choosing appropriate sections, however there are few options as heel strike was the only other consistently observed Poincaré section, and was found to be corrupted by perturbations at certain phases.

It is possible that the PRC was found to be zero because the perturbation applied was too weak to produce a large enough kinematic disturbance. However, this is unlikely as the magnitude used for the ankle torque perturbation was as large as possible while still remaining tolerable by subjects, determined by many iterations of the experimental protocol. The plantarflexion torque pulse seems to delay heel strike when applied just before heel strike, which elicits a sensation of surprise in subjects. The neural controller may be expecting heel strike feedback at a certain time, or state of the body, and when this feedback is not present it triggers a startle reflex. Although this effect was not studied, it provides ideas for experiments to study the neural controller's feedback requirements.

A final possibility is that no phase resetting was observed due to the speed constraint of the treadmill. If this were true, then a comparable experiment conducted over ground might show a

non-zero PRC, due to some difference in the neural controller. The study reported here did not investigate the possible differences between treadmill and over ground walking.

### **4.3 Interpretation of a Zero PRC for Human Walking**

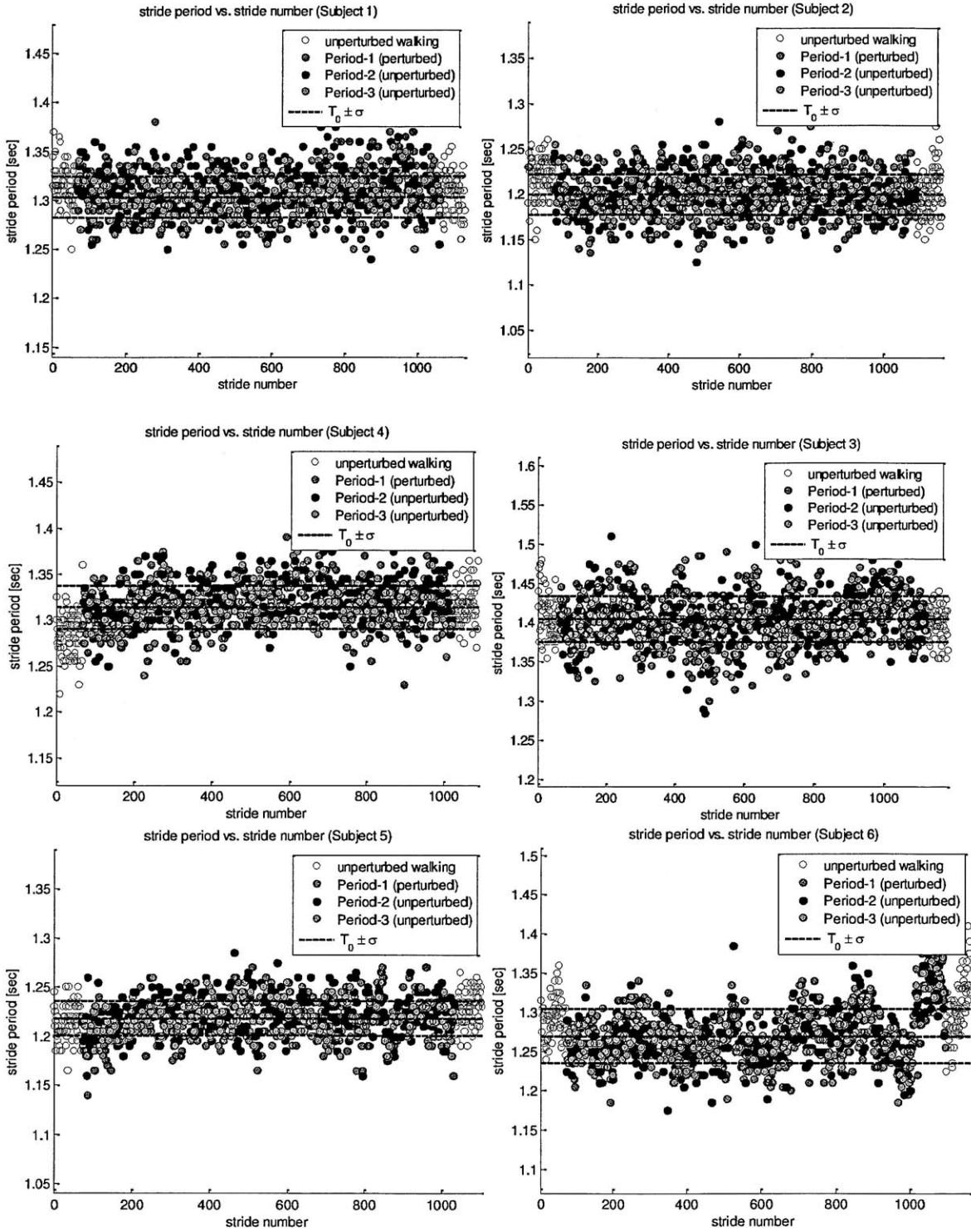
After considering the alternatives above, the clear conclusion from this experiment is that the PRC is zero. Since the knee angle was clearly perturbed off its nominal trajectory (see Appendix B: Knee plane plots sorted by perturbation phase), this suggests that some higher level of neural control may be correcting for the perturbed gait to produce zero phase shift. Which leg is responsible for the corrective action to maintain the phase cannot be determined, since this experiment did not collect data for the behavior of the contralateral leg, which undergoes a full stride during the two periods of settling. This evidence of zero phase resetting is consistent with other convincing evidence for some form of kinematic control of the lower limb; during walking under reduced gravity via a body weight support system, the kinematic coordination of the lower limb was found to be highly repeatable drastic changes in kinetic parameters (Ivankeno, Grasso, Macellari, & Lacquaniti, 2002). For the upper limb, it is well established that the central nervous system utilizes kinematic control to generate maximally smooth trajectories in reaching movements (Flash & Hogan, 1985), thus the ability to control kinematics of the leg, and more specifically the foot, certainly exists.

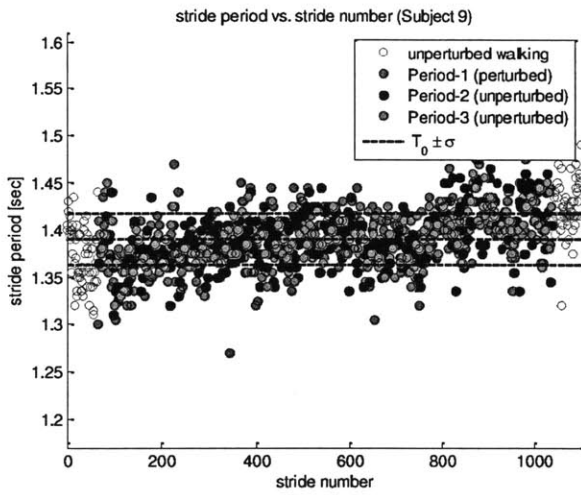
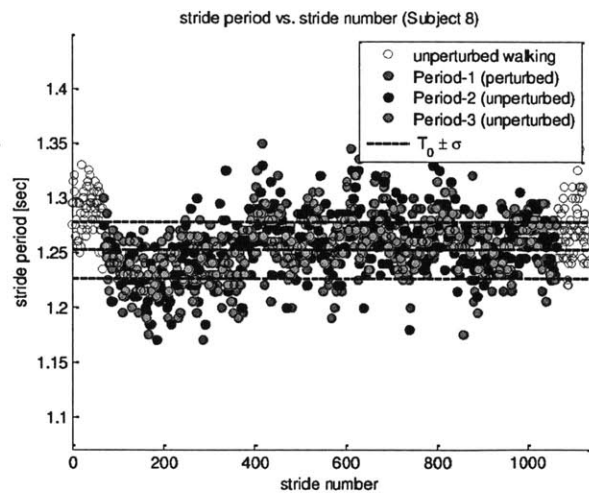
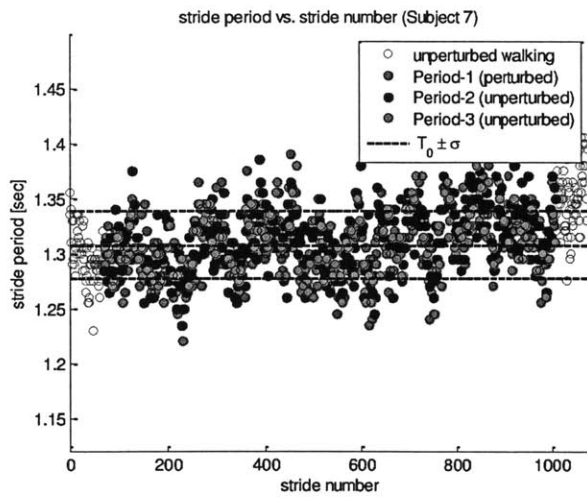
## Bibliography

- Ahn, J., & Hogan, N. (2010). Feasibility of Dynamic Entrainment with Ankle Mechanical Perturbation to Treat Locomotor Deficit. *32nd Annual Intern. Conf. of the IEEE EMBS*, (pp. 3422-3425). Buenos Aires.
- Ermentrout, G. B. (2010). *Mathematical Foundations of Neuroscience*. New York, NY: Springer.
- Feldman, A., Krasovksy, T., Banina, M., Lamontagne, A., & Levin, M. (2010). Changes in the Referent Body Location and Configuration may Underlie Human Gait, as Confirmed by Findings of Multi-Muscle Activity Minimizations and Phase Resetting. *Experimental Brain Research*, 210, 91-115.
- Flash, T., & Hogan, N. (1985). The Coordination of Arm Movements: An experimentally Confirmed Mathematical Model. *The Journal of Neuroscience*, 5(7), 1688-1703.
- Galan, R. F., Ermentrout, G. B., & Urban, N. N. (2005). Efficient Estimation of Phase-Resetting Curves in Real Neurons and its Significance for Neural-Network Modeling. *Physical Review Letters*(94), 158101.
- Ivankenko, Y. P., Grasso, R., Macellari, V., & Lacquaniti, F. (2002). Control of Foot Trajectory in Human Locomotion: Role of Ground Contact Forces in Simulated Reduced Gravity. *J. Neurophysiology*, 3070-3089.
- Nomura, T., Kobayashi, M., & Kozuka, J. (1998). Coordinated Responses of Limb Movement during Human Bipedal Locomotion to External Perturbation. *Proc. of the 20th Annual Intern. Conf. of the IEEE EMBS*, (pp. 2422-2425). Hong Kong.
- Oprisan, S., Prinz, A., & Canavier, C. (2004). Phase Resetting and Phase Locking in Hybrid Circuits of One Model and One Biological Neuron. *Biophysical Journal*, 2283-2298.
- Perry, J. (1992). *Gait Analysis*. Thorofare, NJ: SLACK Incorporated.
- Pikovsky, A., Rosenblum, M., & Kurths, J. (2001). *Synchronization*. Cambridge, UK: Cambridge University Press.
- Roy, A., Krebs, H. I., Williams, D. J., Bever, C. T., Forrester, L. W., Macko, R. M., et al. (2009). Robot-Aided Neurorehabilitation: A Novel Robot for Ankle Rehabilitation. *IEEE Trans. on Robotics*, 25(3), 569-582.
- Smeal, R. M., Ermentrout, G. B., & White, J. A. (2010). Phase-response Curves and Synchronized Neural Networks. *Phil. Trans. R. Soc. B*, 365, 2407-2422.
- Strogatz, S. H. (1994). *Nonlinear Dynamics and Chaos*. Cambridge, MA: Perseus Books Publishing.

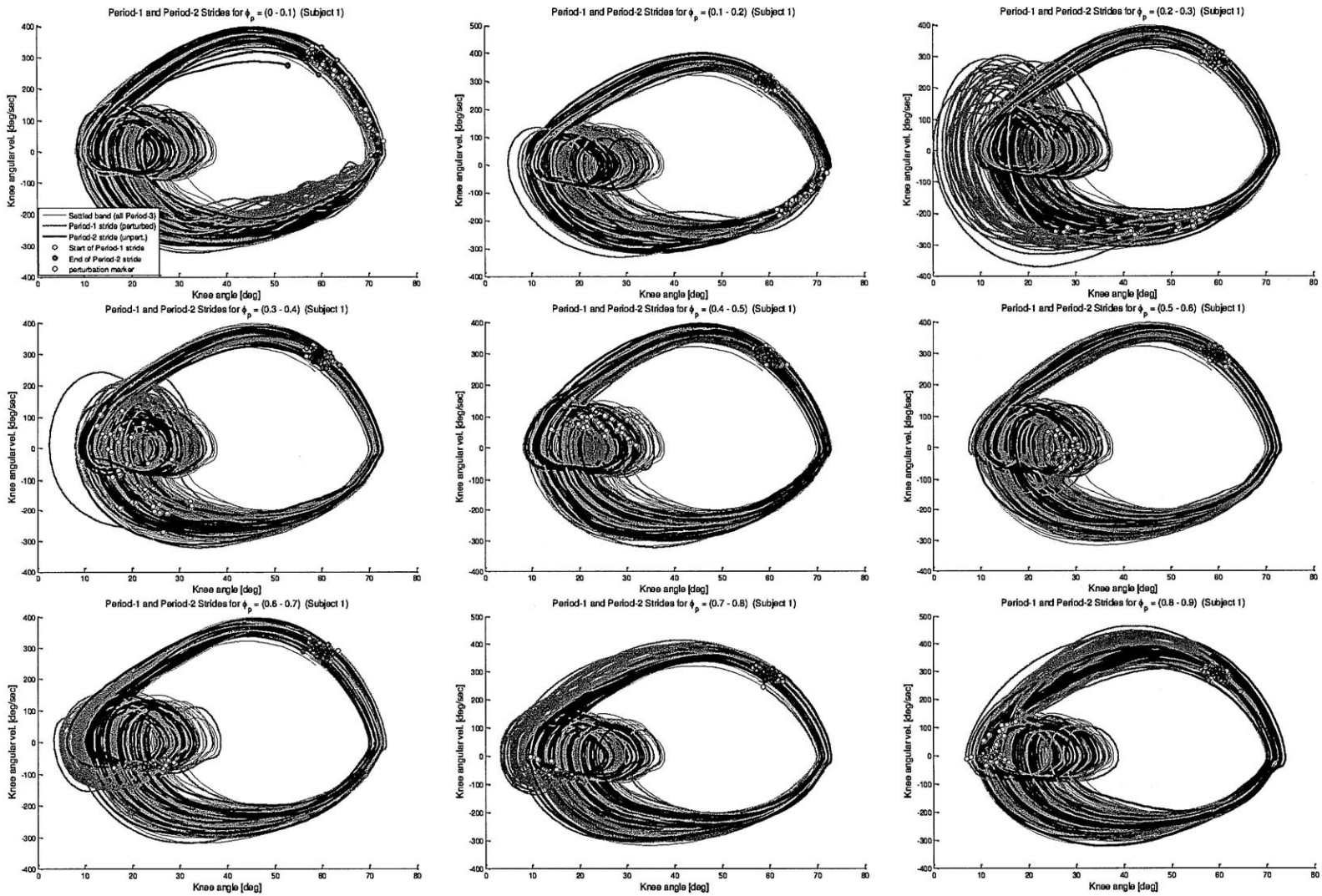
Winfree, A. T. (2001). *The Geometry of Biological Time*. New York, NY: Springer.

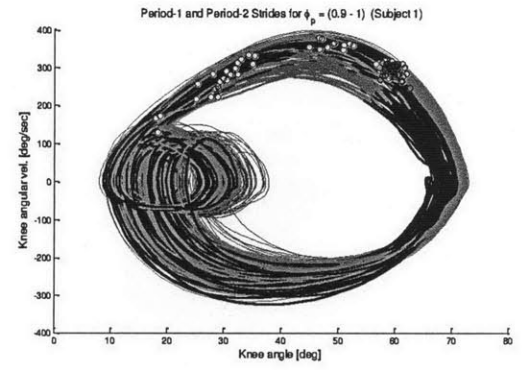
# Appendix A: Stride Periods Plots

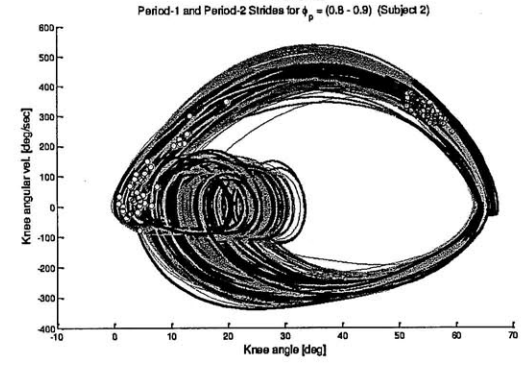
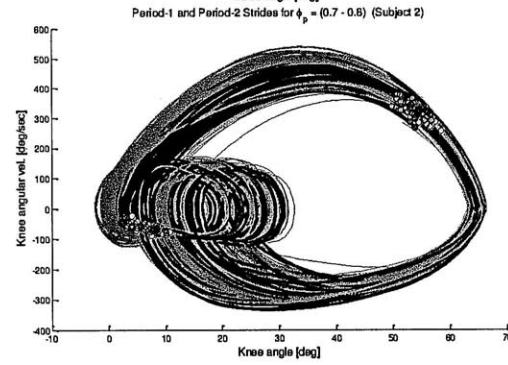
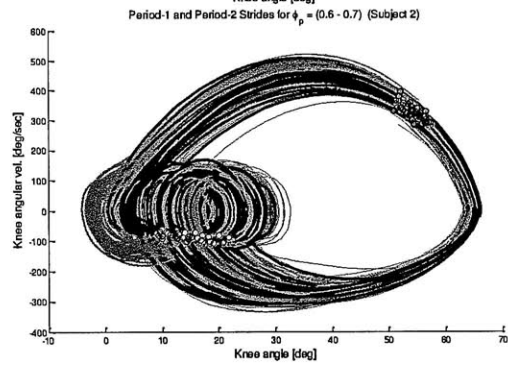
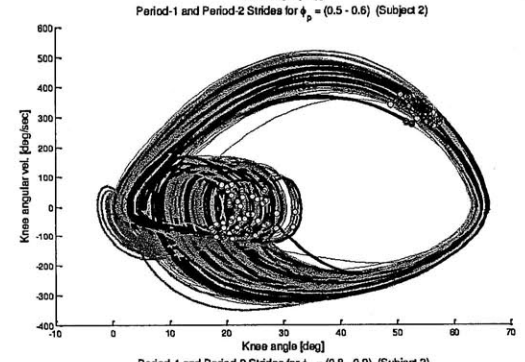
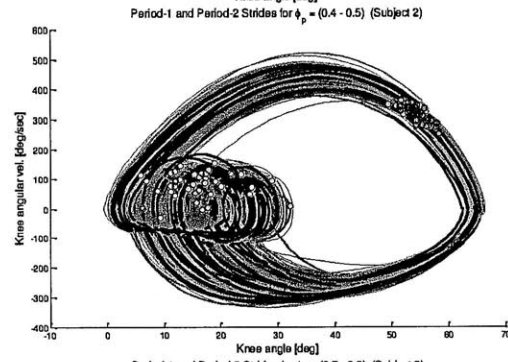
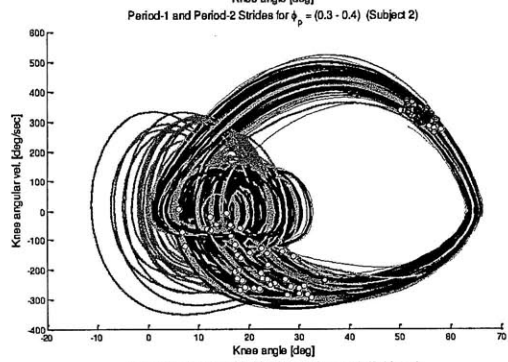
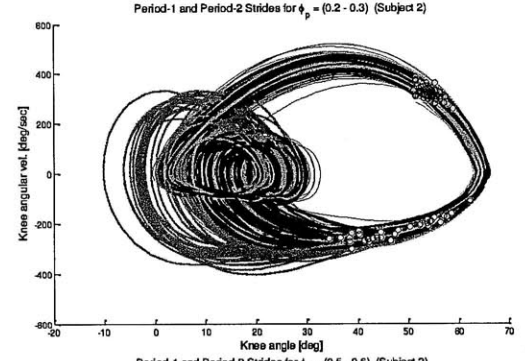
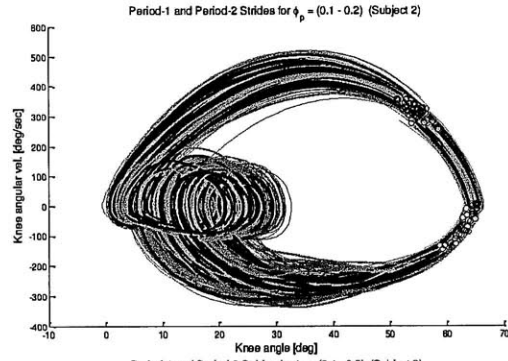
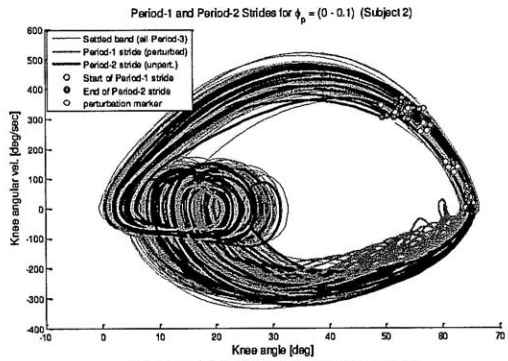


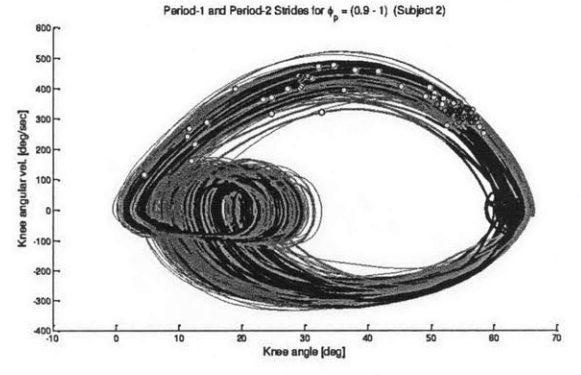


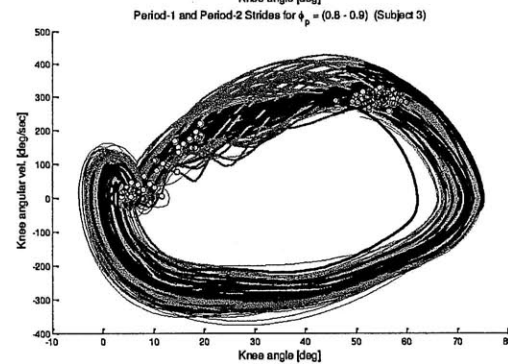
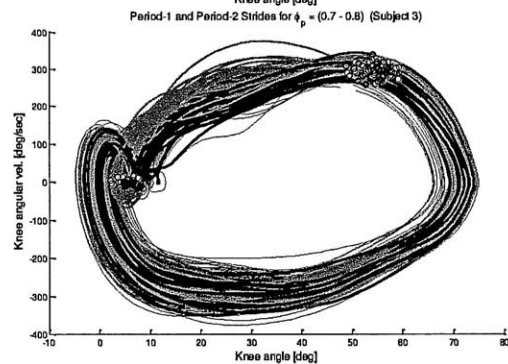
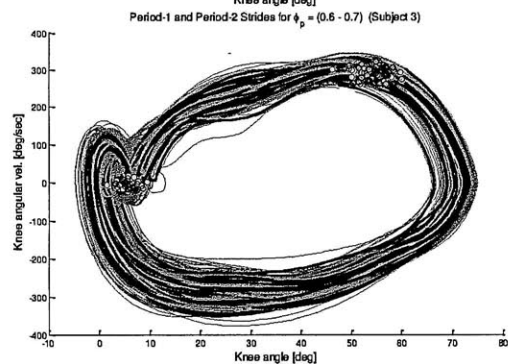
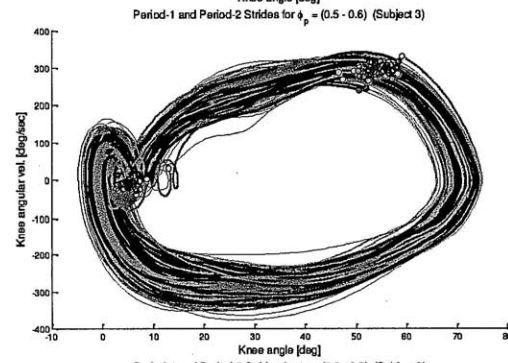
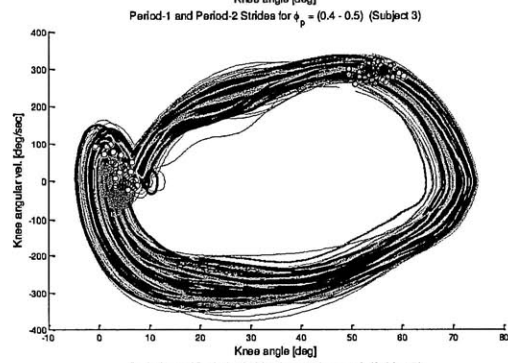
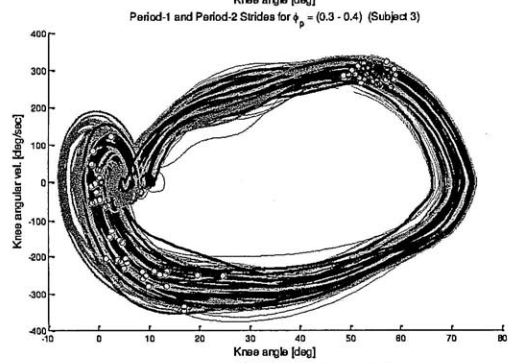
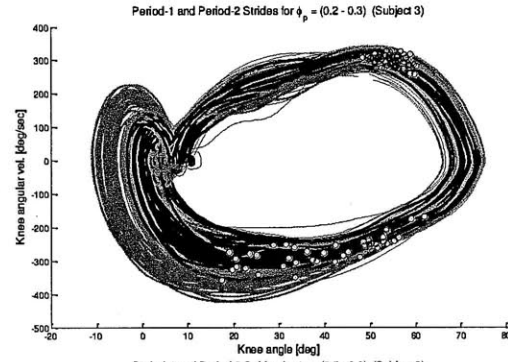
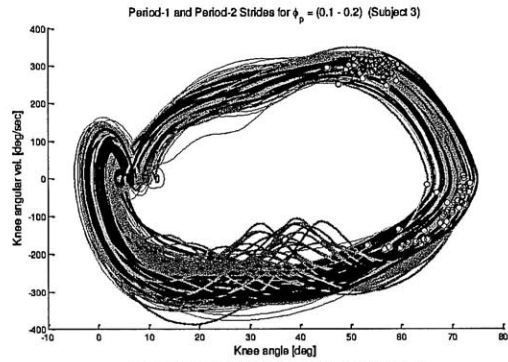
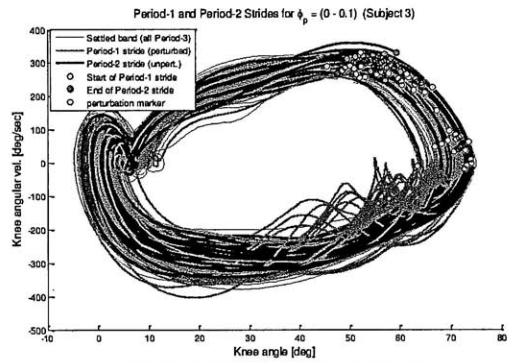
Appendix B: Knee plane plots sorted by perturbation phase

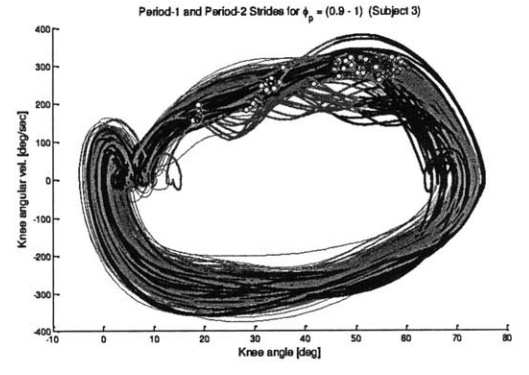


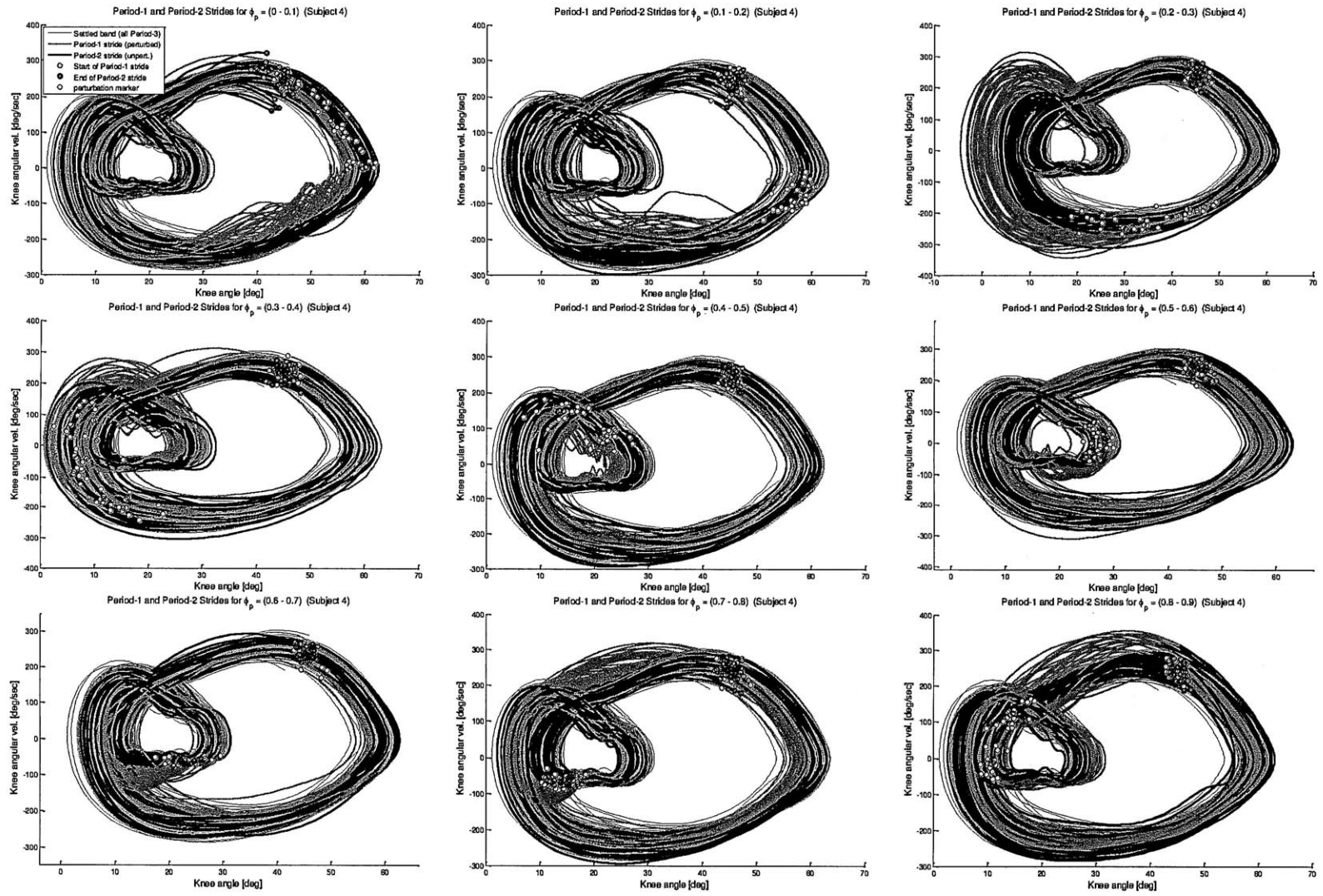


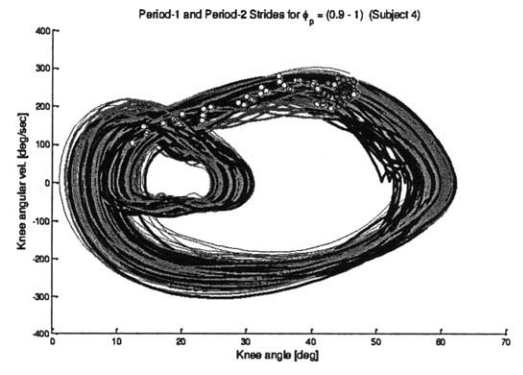


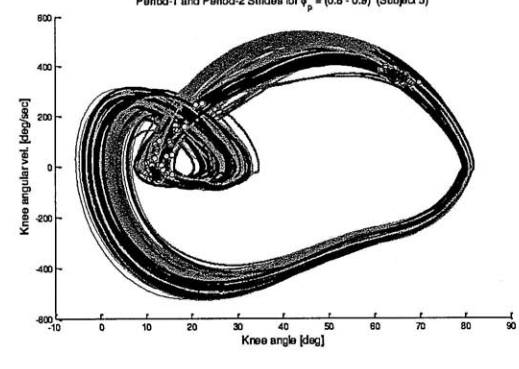
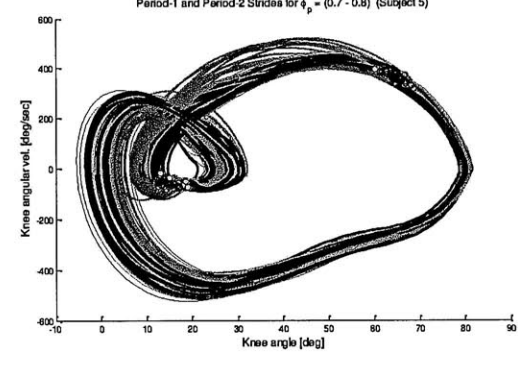
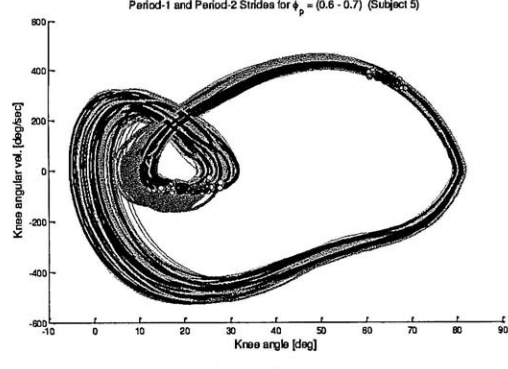
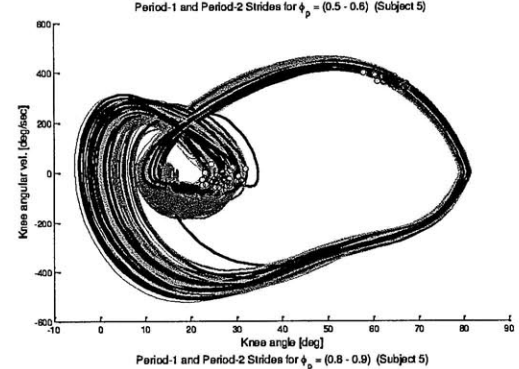
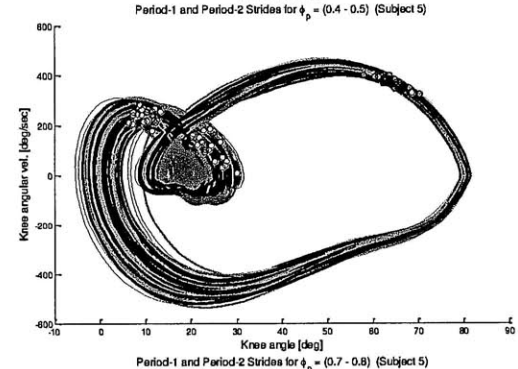
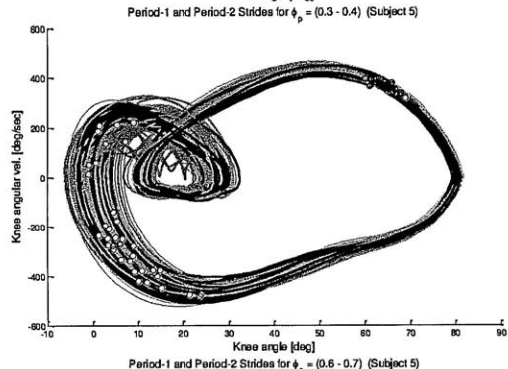
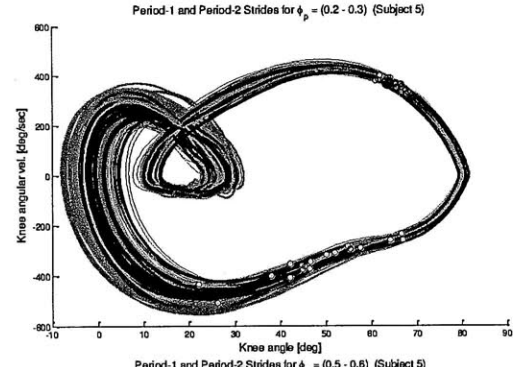
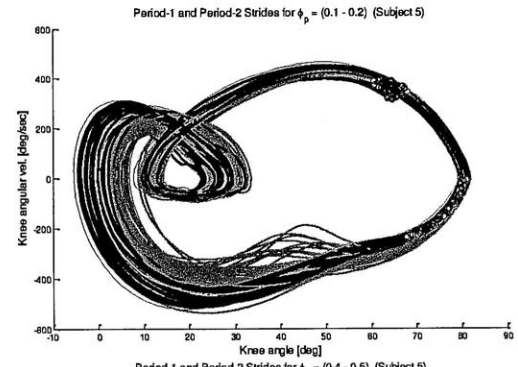
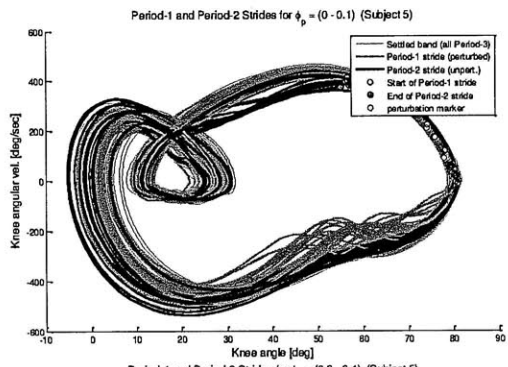


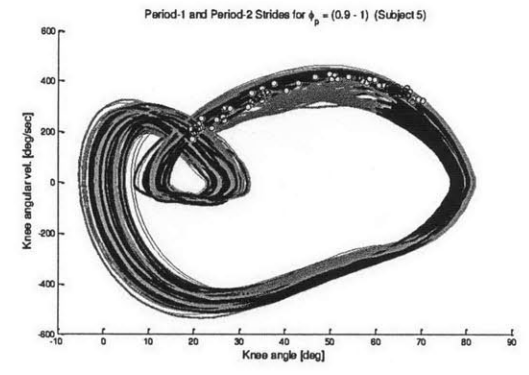


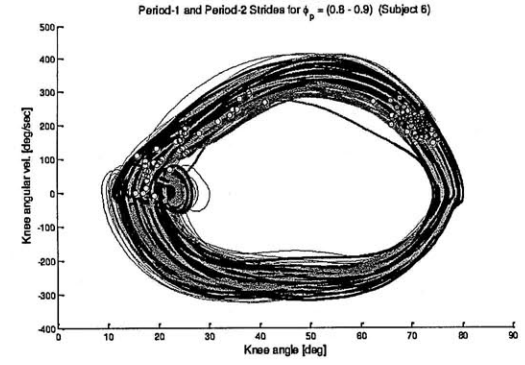
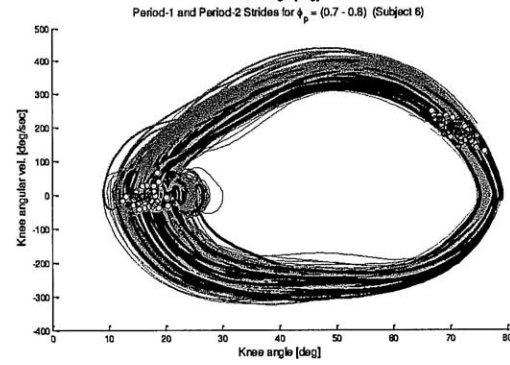
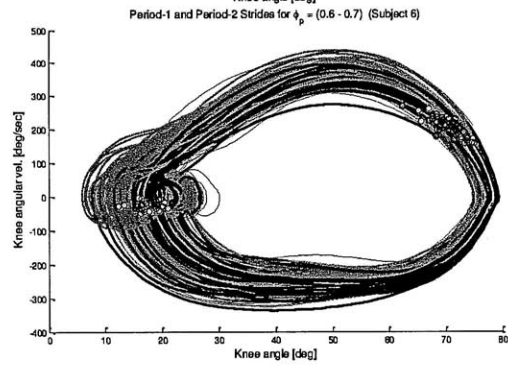
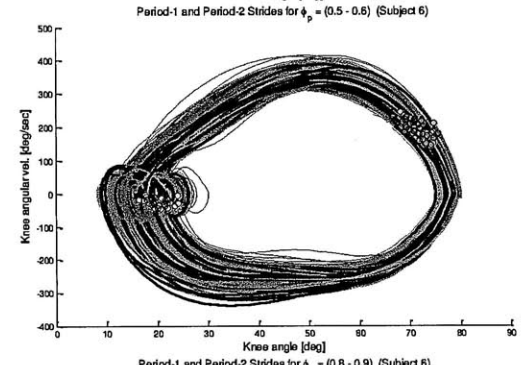
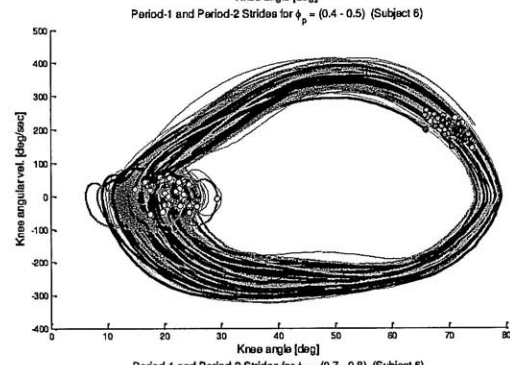
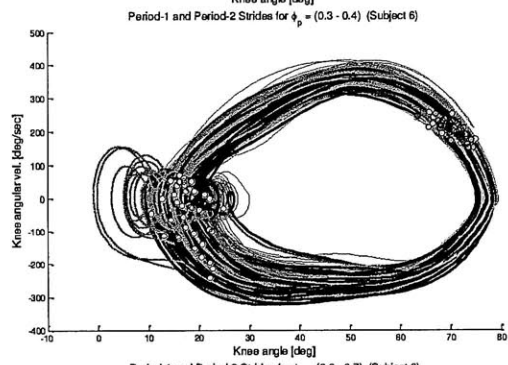
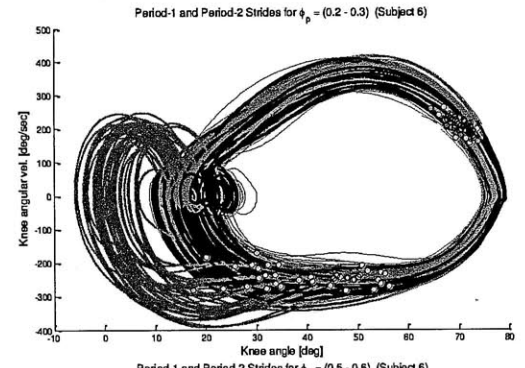
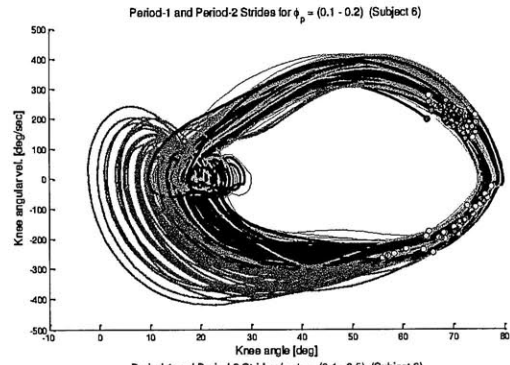
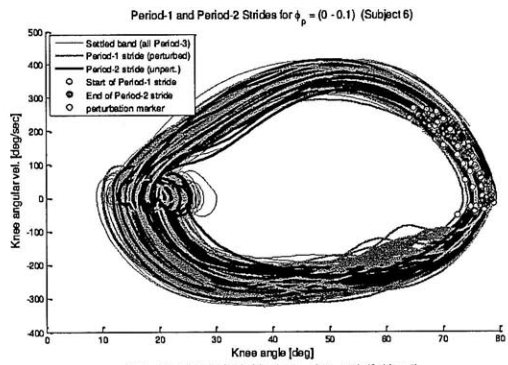


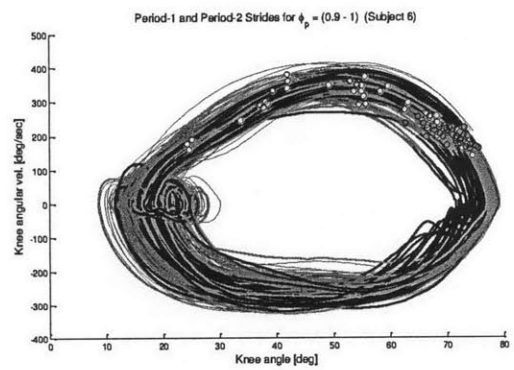


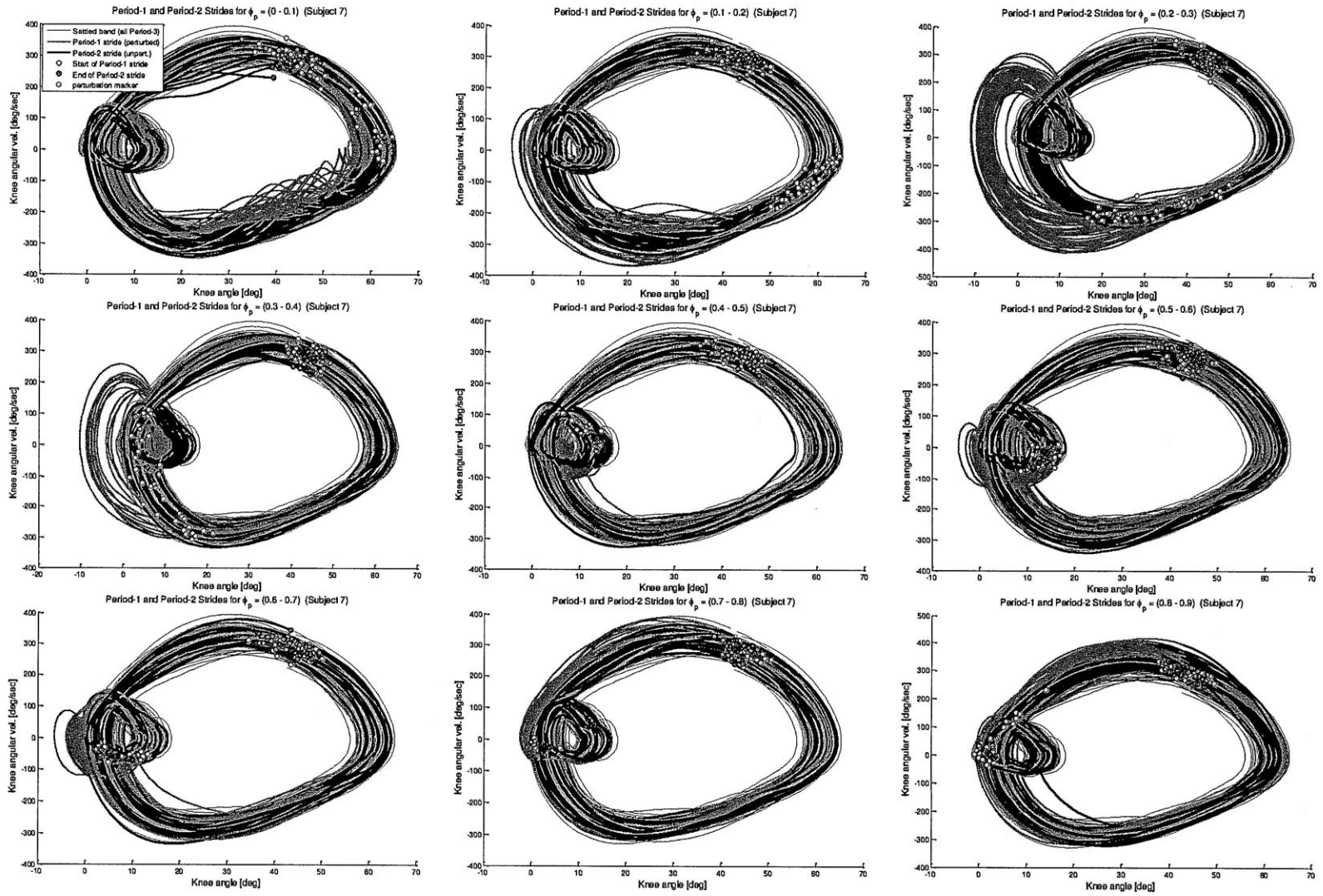


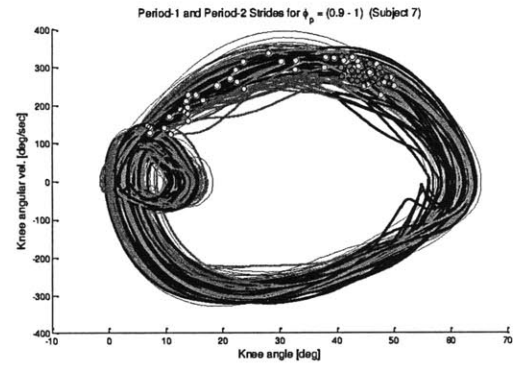


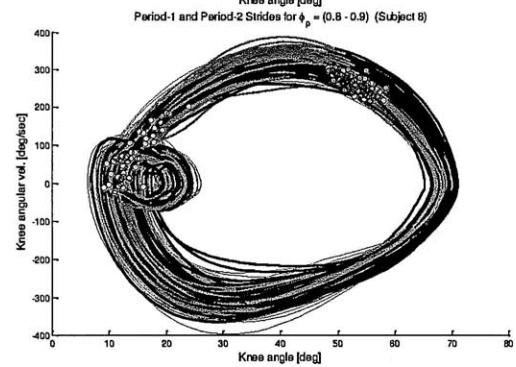
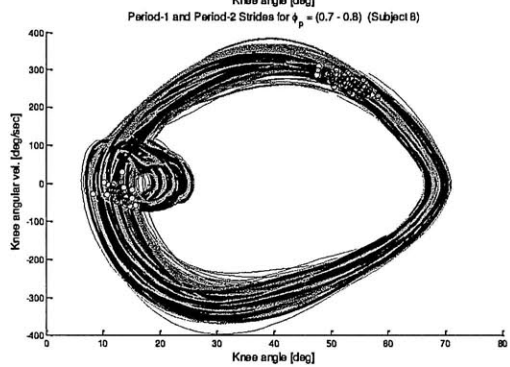
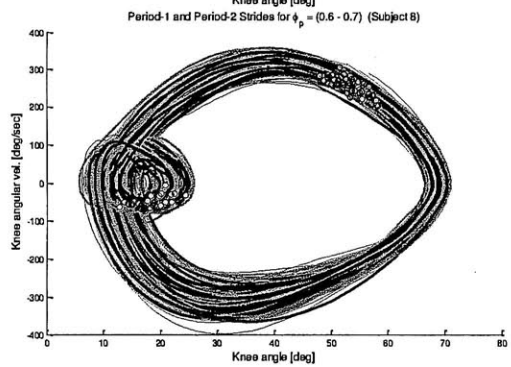
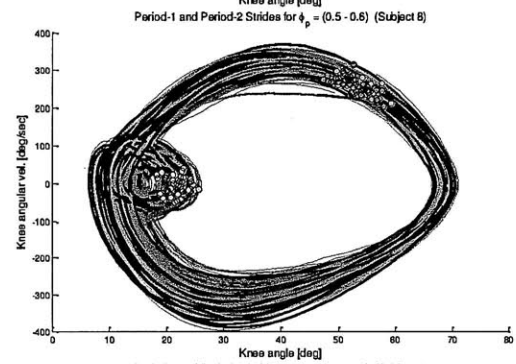
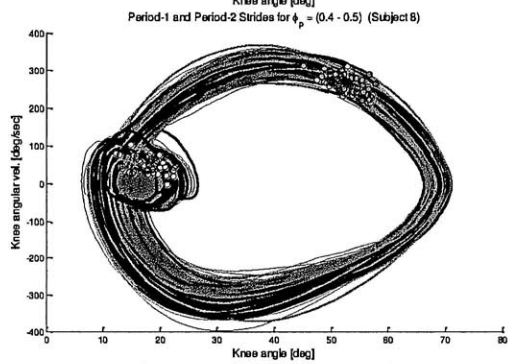
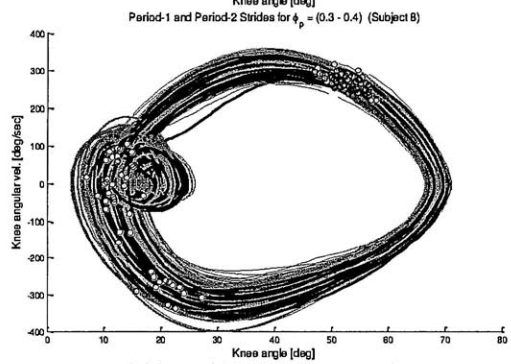
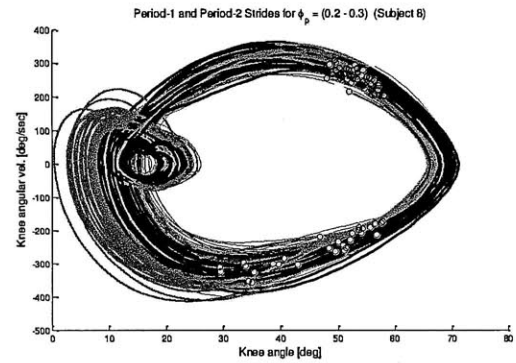
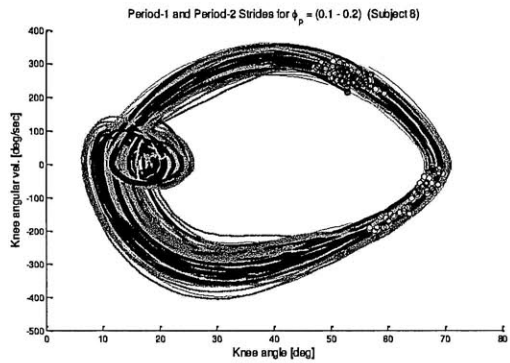
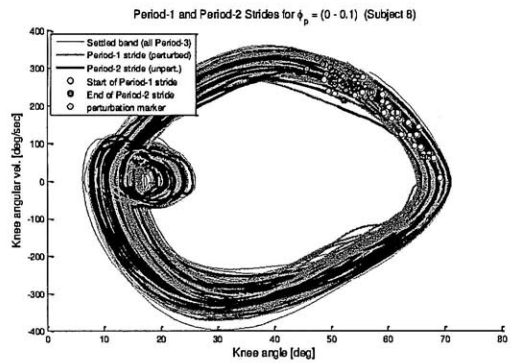


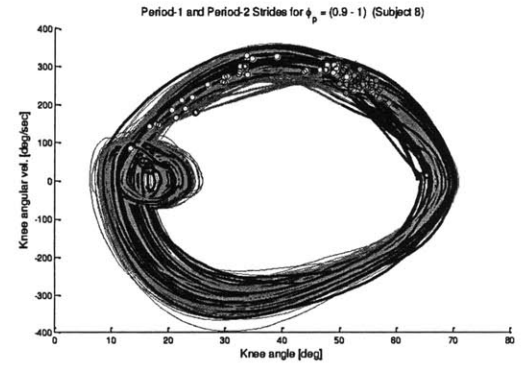


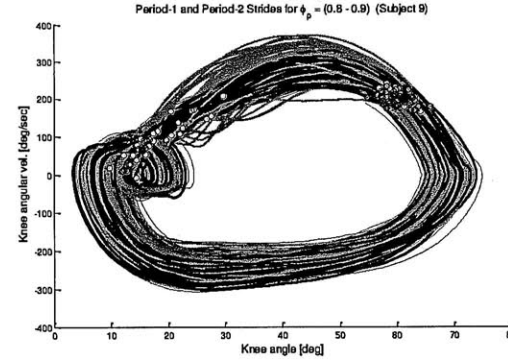
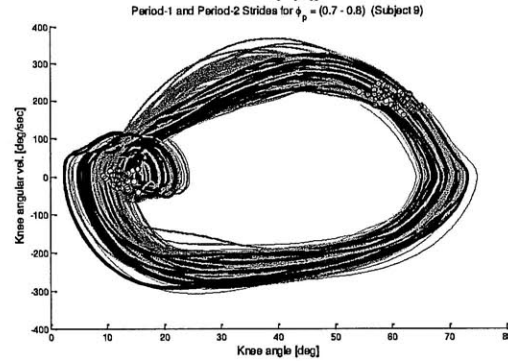
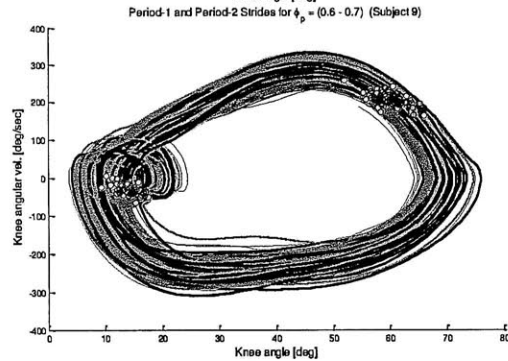
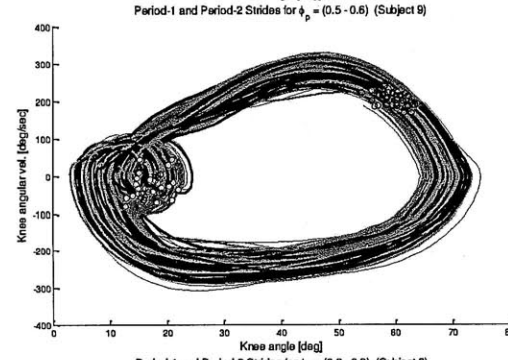
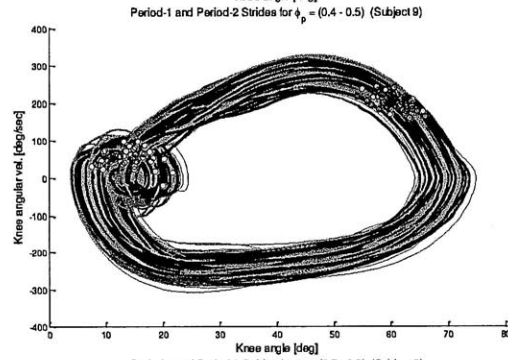
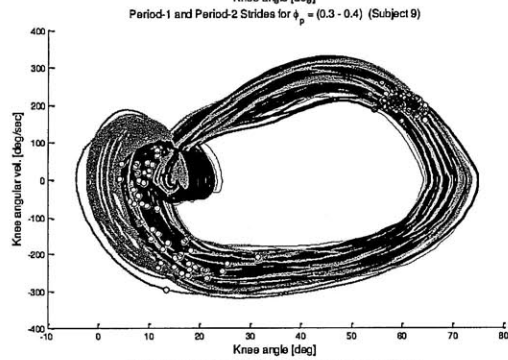
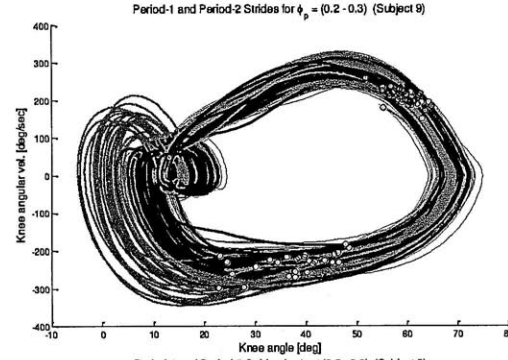
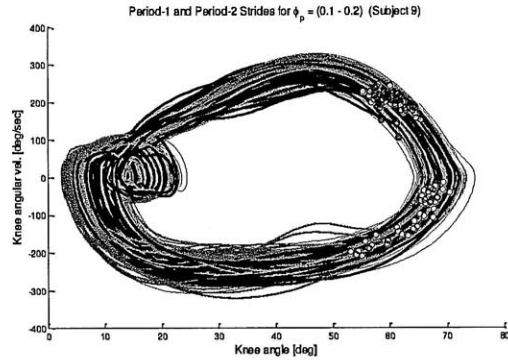
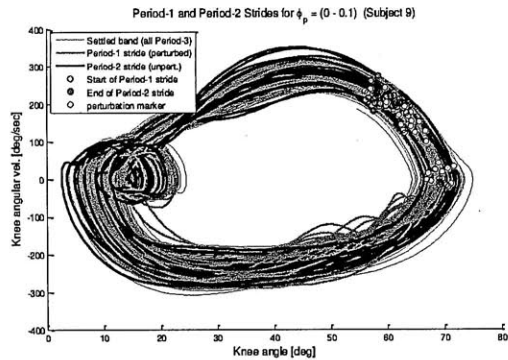


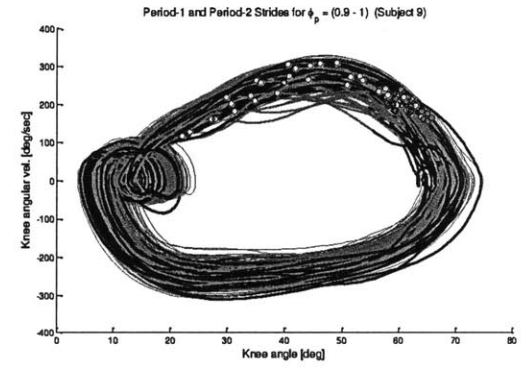




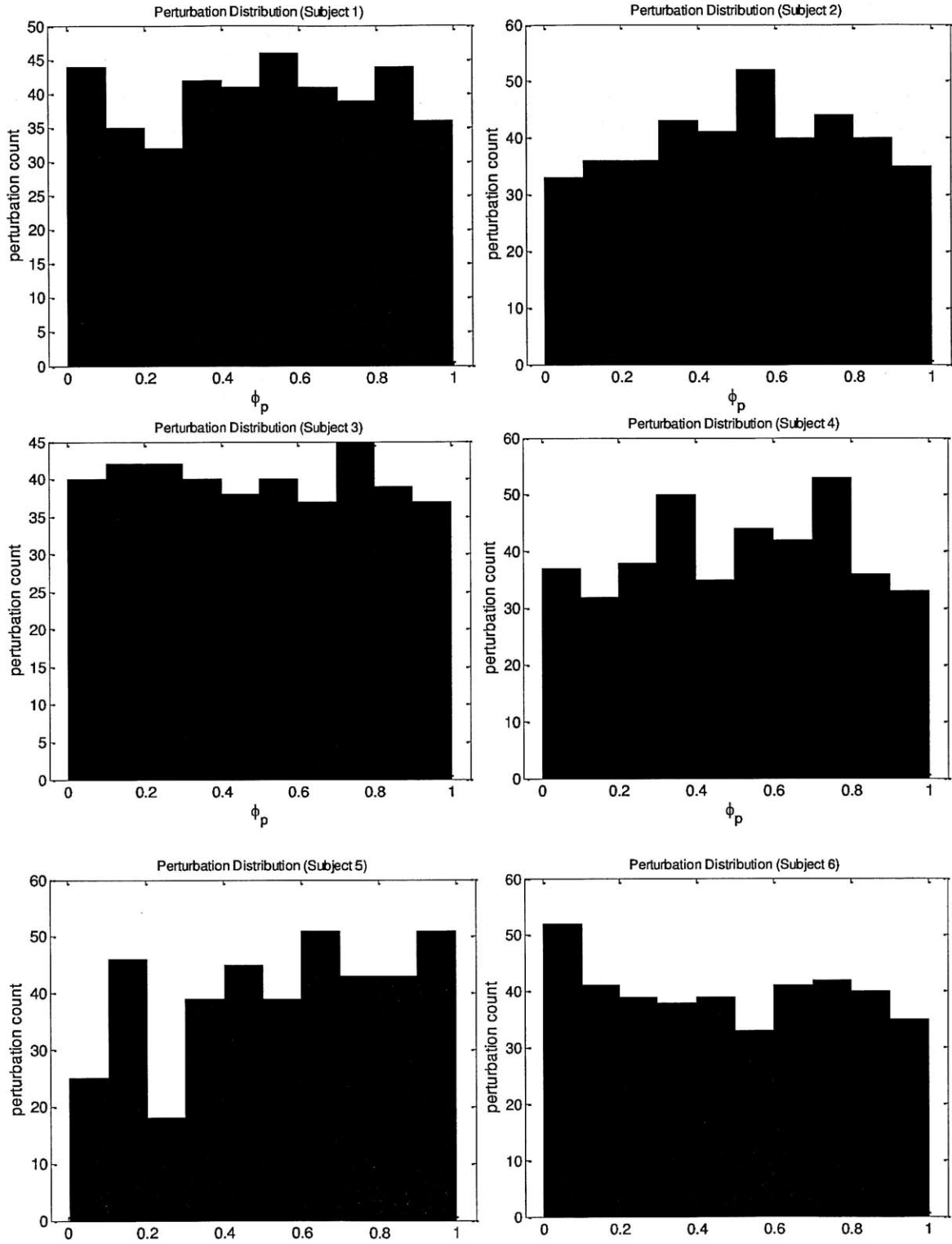


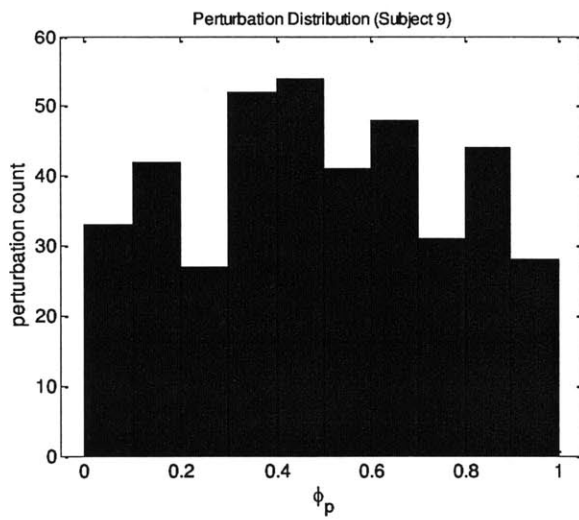
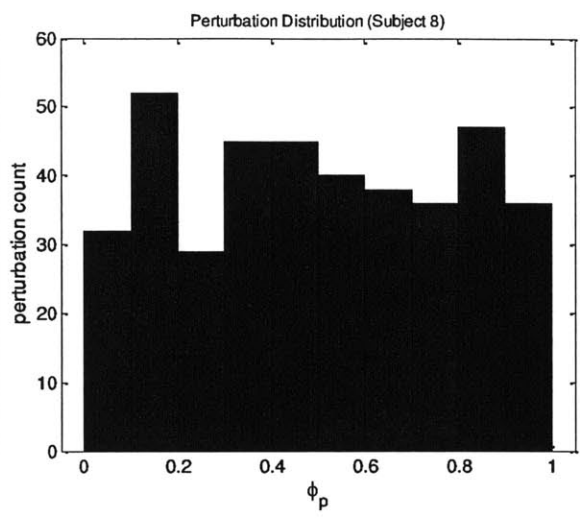
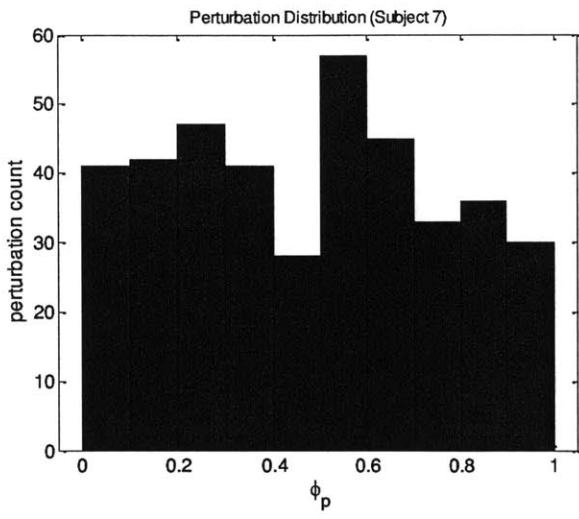






## Appendix C: Histograms of perturbation distributions





## Appendix D: Regression residuals ( $h = 10$ )

